The Layered Oxides in Lithium and Sodium-Ion Batteries: A Solid-State Chemistry Approach

Claude Delmas, Dany Carlier, Marie Guignard

Special Issue Invitations aenm.202000321 (handling editor: John Uhlrich)
In Honor of Nobel Laureate John B. Goodenough

The layered oxides in lithium and sodium-ion batteries: a solid state chemistry approach

Claude DELMAS, Dany Carlier and M. Guignard

Institute of Condensed Matter Chemistry of Bordeaux
CNRS, Univ. Bordeaux, Bordeaux INP, ICMCB UMR 5026, F-33600 Pessac, France

Corresponding author
claude-henri.delmas@icmcb.cnrs.fr

Abstract

This paper gives an overview of the researches carried out on lithium and sodium layered materials as positive electrodes of lithium(sodium)-ion batteries. It is focused on the solid-state chemistry contribution to discover new materials and to optimize the properties vs the requirements imposed by the applications. Among, all material structures, which are considered, the layered one (lithium based), is up to now the best one to have high energy density batteries for mobile applications. Recently, the homologous Na materials, which have lower energy, were considered for stationary applications due to their low price. Starting for $LiMO_2$ materials or Na_xMO_2 ($0.5 < x < 1$) many substituted phases, obtained by high temperature solid state chemistry, have allowed stabilizing the layered structure in large composition domains to increase the specific capacity, which is directly related to the number of exchanged electrons during the cycling process.

1. Introduction

From the discovery of lithium intercalation in TiS_2 by Whittingham[1,2], Steele[3], Murphy[4] and polymer battery by Armand[5] a considerable work was devoted to layered oxides. The archetype of the material used in lithium-ion batteries is $LiCoO_2$, synthesized in 1958. [6] It was considered as positive electrode material for a lithium battery by Goodenough[7] in 1980. Simultaneously, in Bordeaux, we made the first electrochemical study in the Na_xCoO_2 layered oxide[8], which was obtained for the first time by Fouassier[9] in 1972. The introduction of Lithium-ion batteries in 1989 by Sony, with $LiCoO_2$ as positive electrode and a carbon derivative at the negative electrode, promoted Li_xMO_2 layered oxides to be used as positive electrode material. One has to mention here the contribution of Yoshino who made, in 1985, a pioneer work on the lithium intercalation in carbon based materials. [10]

$LiNiO_2$ as positive electrode was first proposed by Dahn in 1990[11,12], then many studies were reported by Ohzuku[13,14] and our group in Bordeaux. [15-17] One of the main problems of $LiNiO_2$ results from its departure from the ideal stoichiometry (presence of nickel in the Li layer) which leads to a large irreversible capacity. We have shown that the substitution of Ni by Co allows obtaining a strictly layered material[18]. Many other cationic substitutions: Mn[14,19,20], Fe[21] were carried out to try to have a better knowledge of this material family and to improve the electrochemical performances. Ohzuku obtained a very important result, concerning the thermal stability of the deintercalated material. He showed that the partial substitution of Ni by Al[22-24] or (Co + Mn) [25,26] makes safer the battery vs pure $LiNiO_2$. From this original work, Chowdary proposed the $LiNi(Co,Al)O_2$ system[27] and Broussely et al. optimized this material for prototype cells[28]. A systematic study of this material family was made by Ukyo who developed a new material $LiNi_{0.8}Co_{0.15}Al_{0.05}O_2$ (NCA) [29,30] which is now used in particular in EV, HEV and PHEV. With Ikuhara, he showed for the first time by high-resolution electron microscopy that a thin layer of rocksalt phase was formed at the surface and at the grain boundaries upon cycling[31]. For a few years, under the pressure of car manufacturers, the Ni rich layered materials have been intensively revisited to try to optimize their electrochemical properties. Most of the researches concern the addition of small amounts of dopants or coatings. Almost all elements are now systematically tested to try to improve the specific capacity and decrease of the fading upon cycling.

Sodium layered oxides as positive electrode materials were intensively studied in Bordeaux in the 80's. The first study on the Na_xCoO_2 system[8] was extended to Ti[32], Cr[33], Ni[33], Mn[34], and mix systems (Ni,Co).[35] The Na_xMoO_2 system was reported by Tarascon in 1986.[36] When Sony commercialized the first Li-ion Battery, all researches moved to lithium batteries. Almost all lithium based positive electrode materials have now been discovered, most of the researches concerns the material optimization and the characterization of the phenomena occurring during the cycling. In 2005-2008 some researchers focused their researches on sodium layered materials. Komaba, after a one year stay in Bordeaux, worked on sodium systems and discovered very promising materials. [37,38] He was followed by many researchers who made interesting reviews[39-45]. Even if the sodium batteries cannot compete with the Li ones for specific energy, for stationary applications they are very promising thanks to the material availability and their low price.

The starting materials are always synthesized by high temperature solid-state chemistry. During the battery charge, the alkali ions are deintercalated and re-intercalated during the discharge. The highly deintercalated materials are metastable. Their structure can change by slab gliding or by

cation migration from the slab to the interslab space. Jahn-Teller distortion can also occur. Depending on the cations and of their oxidation states the electronic conductivity, which is a key parameter for the kinetic of the process, can change of several orders of magnitude. The material stability in the deintercalated state is a very important parameter concerning the safety. A thermal decomposition at intermediate temperature can lead to oxygen evolution and to a battery runaway. A solid-state chemistry approach considering: (i) the relative stability of the various oxidation states, (ii) the crystal field stabilization, (iii) the occurrence of structural distortions, (iv) the tendency to cation ordering and the sensitivity to water is required to understand the various phenomena and to optimize the materials for applications. In this review, the issue of particle texture and coatings, which are essential for applications, are out of the topic of the paper. Nevertheless, one has to note the very important contribution of Sun team who optimized in several steps, the particle texture and the composition of Li(Ni,Mn,Co)O_2 (NMC) based materials to keep a very high capacity, with an improved stability at high voltage and reduced crack formation. He proposed successively the Core-Shell Concentration Gradient (CSG) [46], the Full Concentration Gradient (FCG) [47] and the Two Slopes Full Concentration Gradient (TSFCG) [48] with increasing performances.

2. Layered oxides overview

Layered oxides exhibit the A_xMO_2 formula (A = Li, Na; M = transition metal element). Their structure is made of MO_2 slabs, built of edge-sharing MO_6 octahedra, separated by a layer of Li^+ or Na^+ ions. These materials crystallize generally in the hexagonal system (or rhombohedral). In some case if M is a Jahn-Teller ion (Ni^{3+} or Mn^{3+}) a macroscopic distortion can occur leading to a monoclinic or an orthorhombic phase. The $a_{hex.}$ parameter is equal to the M-M intra-slab distance, whereas the $c_{hex.}$ parameter is a multiple of (2, 3, 4, 6 …) of the interslab distance perpendicular to the slabs. Figure 1 gives a schematic representation of the structure of a layer material. The bonds in the MO_2 slabs have an iono-covalent character that plays an important role on the electronic properties. Depending on the alkali metal content an electronic conduction occurs either by hopping (semi-conductor) or by delocalization (metallic-like). The electronic conduction depends on the nature of the M cation: (i) occupation of the t_{2g} or e_g levels, (ii) M-M bond distance vs the t_{2g} orbital extension, (iii) average oxidation state, (iii) presence of Jahn- Teller effect. On the opposite, the A-O bonds are more ionic, the A^+ ions can move in the interslab space if there are enough vacancies. The layered structures can be stable within large composition domains, at least at room temperature, for some transition elements. The domain extension depends on the redox potential of the $M^{3+/4+}$ couple and

on the structure stability. The ionic and electronic conductivities and the existence of a large composition domain are the three main requirements for a material to be used as positive electrode material in a secondary battery if the redox couple is enough high.

Most AMO_2 (A = Li, Na) phases exhibit the α-$NaFeO_2$ type structure which derives from the rocksalt one by ordering of alkali ions and transition metal ions along one of the threefold axis of the cubic rocksalt structure. It allows minimizing constraints when the difference in ionic radius is too large. As shown in Figure 2 all sodium $NaMO_2$ phases exhibit the ordered layer structure while in the case of lithium materials, the layered structure is only observed for the smallest trivalent transition elements (M = V, Cr, Ni, Co). For $LiTiO_2$, $LiMnO_2$ and $LiFeO_2$ the difference in size between M^{3+} and Li^+ ions is too small to form the layered structure; they exhibits either a rocksalt or another ordered structure deriving from the rocksalt one.

Whereas in the lithium materials obtained by high temperature solid state chemistry, all oxygen octahedra are fully occupied leading to the $LiMO_2$ formula, the homologous sodium phases can be sodium deficient (Na_xMO_2) ($0.5 < x < 1$). Depending on the synthesis temperature, on the M nature and on the sodium amount, sodium ions can be either in octahedral or in trigonal prismatic environments. Therefore, the oxygen packings are different. These sodium phases can be also used as precursor to obtain, via Li^+/Na^+ exchange, lithium layered oxides that cannot directly be synthesized by classical high temperature solid state chemistry. Figure 3 gives a view of the structure of the three types of structures (O3, P3, P2). Many others structures are metastable (O1 and O2 as example), they can be obtained by alkali metal deintercalation or exchange. To describe these structures in a convenient way, we proposed the following nomenclature: one letter P (for trigonal prismatic), O (for octahedral) or T (tetrahedral) is used to define the alkali ion site, whereas a figure (1, 2 or 3) is used to indicate the number of MO_2 slabs within the hexagonal cell (in most cases the unit cell can be described in the hexagonal system). [49] If a structural monoclinic or orthorhombic distortion occurs a prime (') is added in the designation. If a triclinic distortion occurs a double prime ('') is added. All $LiMO_2$ layered phases exhibit the O3 type structure. In the 3d series most of the $NaMO_2$ phases (M = Ti, V, Cr ,Fe, Co) exhibit the O3 type structure (R-3m) while $NaMnO_2$[50] and $NaNiO_2$[51] crystallize in the monoclinic system (C2/m) thanks to the Jahn-Teller effect of Mn^{3+} and Ni^{3+} ions. Therefore, their structure is designed as O'3. The Na_xMO_2 materials obtained by solid state chemistry exhibits the P3 structure (R-3m) for a composition close to $Na_{0.5\text{-}0.6}MO_2$ and the P2 one ($P6_3/mmc$) for higher Na amounts ($Na_{0.6\text{-}0.8}MO_2$). [9]

Due to the 2D character of the structure, the MO_6 octahedra are flattened along the threefold axis, while the AO_6 polyhedra are expanded. The same phenomena occurs in materials with trigonal prismatic sites, but in these cases, there is face-sharing between MO_6 octahedra and AO_6 trigonal prisms. In the case of the P3 structure, each AO_6 prism shares one face with one MO_6 octahedron on one side and 3 edges with 3 MO_6 octahedra on the other side. There is only one type of environment; the Na^+ ions are displaced along the trigonal axis to minimize the electrostatic repulsions. In the case of the P2 structure, two types of sites are present in the interslab space: one shares only edges with the MO_6 octahedra, while the other one shares two faces with the MO_6 octahedra. Due to the vicinity of the two sites, they cannot be occupied simultaneously. The sodium/vacancy distribution depends on the competition between the Na^+/M^{n+} and Na^+/Na^+ interactions. This point be will further discussed.

As shown in Figure 3, in the O3, P3 and O1 structures the MO_6 octahedra have the same orientation; therefore, one packing can be transformed into the other one by slab gliding without any break of the M-O bonds. The gliding can be described by a circular permutation of the A B C positions of a triangular lattice. The O3 $\rightarrow$ O1 transition occurs in the $LiCoO_2$ and $LiNiO_2$ systems (possibly with intermediate phases) when all lithium ions are deintercalated. [52-53] This reaction is completely reversible from the structural point of view, but the change in volume involved hinders a long range cycling. In the O1 structure, the octahedra situated between the MO_2 slabs share faces with the MO_6 octahedra. Therefore, their occupation by Li^+ would lead to really strong cationic repulsion and those octahedra are more likely empty. On the contrary, for the MO_2 composition this packing minimizes the overlapping of oxygen p orbitals through the Van der Waals gap. It must be noticed that the homologous sulfides $LiMS_2$ exhibit the O1 packing as a result of the small ionicity of their bonds. This structure is also observed for $M(OH)_2$ divalent hydroxides, in this case the hydrogen atom is in tetrahedral environment (T1) (no face sharing with MO_6 octahedra). Several intermediates phases can occur due to A^+/vacancy orderings in the $0 < x < 1$ range. In the case of the Na phases the O3 $\rightarrow$ P3 transition occurs upon partial Na deintercalation from the O3-$NaMO_2$ phase; it is completely reversible upon Na re-intercalation. On the contrary, in the P2 structure there are two types of octahedra orientation. Therefore, it is impossible to obtain the O3 or P3 structure by slab gliding from the P2 structure. In the Li_xMO_2 systems, the small size of the lithium ions prevents from them occupying trigonal prismatic sites.

Sodium derivatives with trigonal prismatic environment can be used as precursor to obtain metastable lithium phases. Starting from an O'3-$NaMnO_2$ phase, an O'3-$LiMnO_2$ phase was obtained

by Li^+/Na^+ exchange.[54,55] This phase is metastable and decomposes above 300°C.[54] One can note the synthesis of O2-$LiCoO_2$ from P2-$Na_{0.70}CoO_2$. [56,57]This new variety of $LiCoO_2$ is very crystallized; it can be used as positive electrode of lithium batteries. [57] The structure of the O2 phase is also given in Figure 3, the LiO_6 octahedra share one face with the CoO_6 octahedra. This material is metastable and it is transformed into the O3-$LiCoO_2$ above 250°C. A similar approach was carried out by Dahn and Paulsen to prepare the Li phase from the $Na_xMn_{2/3}Ni_{1/3}O_2$ system.[58] Moreover, his team succeeded for the first time in obtaining the fully deintercalated phase O2- $Mn_{2/3}Ni_{1/3}O_2$ phase[59]. The OP4 $Na_{0.42}Li_{0.42}CoO_2$ exhibits an alternation of Li and Na layers[60,61] (Figure 4). Lithium ions are in octahedral sites while Na^+ ions are in trigonal prismatic sites. When Li^+ ions are exchanged to Na^+, there is a slab gliding that transform the trigonal prisms in octahedra (O4 packing). [62,63] Like in the O2 structure, the O4 phase is metastable as a result of the face sharing between CoO_6 and LiO_6 octahedra that reduce the thermal stability.

3. The Li_xMO_2 systems M = 3d cations

The four $LiMO_2$ layered phases, which can be obtained by solid state high temperature chemistry (M = V, Cr, Ni, Co), crystallize in the hexagonal system (R-3m space group) whereas $LiMnO_2$, which is obtained by exchange from the $NaMnO_2$, crystallize in the C2/m space group (Jahn- Teller effect of Mn^{3+}). Among them, only $LiCoO_2$ and $LiNiO_2$ present an interesting electrochemical behavior with a good reversibility of the deintercalation/intercalation process. In the case of $LiVO_2$, one part of the vanadium move irreversibly to the lithium layer upon deintercalation. [64] The migration of manganese atoms to the lithium layer is also observed in $LiMnO_2$ obtained by Na^+/Li^+ exchange and the structure of this phase is irreversibly transformed into spinel during the first cell charge.[65,66] In all Li_xMO_2 systems, during the deintercalation the layered structure becomes unstable due to the anisotropy of the bonds distribution: there is formation of very covalent MO_2 slabs whereas the interslab space becomes empty with oxygen layers face to face. Therefore, there is a tendency to a cationic displacement to homogenize the charge distribution. This leads to a cation migration to the lithium layer. To achieve this cationic transfer the transition metal ions have to move through a tetrahedral interstitial site. At this state, the crystal field stabilization plays an important role to stabilize cations in the octahedral site and to destabilize it in tetrahedral site, as it was summarized in the recent review of Manthiram. [67] This makes impossible, or difficult, the cation transfer from the MO_2 slab to the interslab space. Low spin (LS) Co^{3+}(d6) and LS Co^{4+}(d5) and LS Ni^{3+}(d7) and LS Ni^{4+}(d6) have a very strong stabilization in octahedral site. In the opposite Ti^{3+}(d1), V^{3+}(d2), have

very low stabilization and can move. Ti^{4+}(d0), Fe^{3+}(d5) and Mn^{2+}(d5) which are not stabilized in octahedra vs tetrahedra move easily. In the case of Mn, the Mn^{3+} ions have a strong tendency to disproportionate into Mn^{4+} and Mn^{2+}. This leads to a Mn^{2+} dissolution into the electrolyte, which is reduced at the negative electrode to Mn and deposited. This stabilization in octahedral sites as also an important effect of the stability of deintercalated material at increasing temperature. This point will be further discussed in the part devoted to battery safety.

3. 1. $LiCoO_2$

The high temperature stable O3-$LiCoO_2$ phase has been used in commercial Li-ion batteries with a graphite negative electrode for 30 years. These batteries are used in almost all portable systems (laptops, cellular phones,….). After the discovery by Goodenough of the electrochemical behavior of $LiCoO_2$ a huge number of studies was carried out on this material. A typical cycling curve of a lithium//Li_xCoO_2 cell is shown in Figure 5. [68] The deintercalation/intercalation is reversible. The small irreversibility observed after the first discharge depends on the cell cycling conditions and also of the exact stoichiometry of the material. The starting $LiCoO_2$ phase is an ionic and electronic insulator: (i) there is no lithium vacancies, (ii) the trivalent cobalt ions are in the low spin state (t_{2g}^6). As soon as the Li deintercalation starts at the particle surface, lithium vacancies appear and allow lithium diffusion. From the electronic point of view, there is formation of Co^{4+} (t_{2g}^5), the small distance between the cobalt ions allows orbital overlapping that induces electronic delocalization. The critical distance can be estimated from the formula proposed by Goodenough. [69] These results were confirmed experimentally by conductivity measurements and ^{7}Li MAS NMR study[70] and theoretically from DFT calculation. [71] For x = 0.50 a small anomaly is detected on the voltage curve. At this composition there is a monoclinic distortion as it was proposed by Dahn[72] and Ohzuku. [73] The Li/vacancy ordering was proved by electron diffraction.[74] This phase crystalizes in the P2/m space group. As shown on Figure 5, the lithium and vacancies are ordered on raws, which are parallel to the [110] direction on the hexagonal sublattice. If all lithium ions are extracted, the CoO_2 phase, which exhibits the O1 packing, is then formed. [52] Due to the presence of two oxygen layers with no cations to screen the O-O repulsions, this structure is very instable. It is irreversibly transformed into Co_3O_4 with oxygen release upon heating. This phenomenon occurs in all very deintercalated layered oxides and it is at the origin of the safety problems of this type of batteries. For the intermediate $Li_{0.16}CoO_2$ composition a new phase with O1 and O3 interslab space is formed. The possible existence of this new phase first named (H1-3) was proposed by Van der Ven and Ceder from

theoretical calculations.[75] Dahn confirmed this result experimentally.[76] The structure is represented on Figure 6. In fact, it must be designed as O6(O1-O3) that indicates the alternation of O1 and O3 type alkali ion layers in the general designation of A_xMO_2 oxides. The mechanism of its formation is not completely understood. One can assume that when the number of lithium ions in the interslab space is too small there is a tendency to form domains with different compositions. This behavior is similar to the stage formation in graphite intercalation compounds (Daumas-Herold domains). [77]

If a Li/Co ratio larger than 1 is used during the synthesis, the structure of the pristine material is slightly modified. [78,79] Some lithium ions occupy the cobalt site leading to the presence of oxygen vacancies for charge compensation. The real material formula is $Li[Li_tCo_{1-t}]O_{2-t}$.[80] The stoichiometric material can be obtained only in very specific experimental conditions with a very long annealing of the over-stoichiometric phase. [81] A systematic study of the phase diagram shown that *t* varies in the 0-0.08 range. Depending on the amount of extra-lithium, the shape of the cycling curve changes continuously. The curves of the first charge of the two phases are compared on Figure 5. The biphasic domain due to the insulator / metal transition observed for the stoichiometric phase is replaced by a continuous variation for the overlithiated phase[68]. In the overlithiated material for x = 0.5, the presence of structural defects in the CoO_2 slabs prevents from the Li/vacancy ordering. On Figure 7 the structural model of the defect is represented. The presence of an oxygen vacancy leads to the formation of square pyramidal surroundings around lithium and cobalt ions. Therefore, the trivalent cobalt is no more in the classical t_{2g}^6 Low Spin configuration but exhibits the Intermediate Spin state configuration (IS-Co^{3+}:d_{xy}^2, d_{yz}^2, d_{xy}^1, d_{z2}^1). [82,83] The presence of unpaired electron in over-stoichiometric $LiCoO_2$ has a strong effect on the ^{7}Li MAS NMR spectrum. Due to its sensitivity, Li NMR is the best method to evidence the presence of Li excess in $LiCoO_2$, which plays a very important role in the electrochemical behavior of $LiCoO_2$ in commercial batteries.

3. 2. Li_xNiO_2 and derivatives

3. 2. 1. Li_xNiO_2

Although, $LiCoO_2$ is the most used positive electrode material in portable device, the cost of cobalt limits its use in large scale battery (HEV, PHEV and EV). The structure similarity between $LiCoO_2$ and $LiNiO_2$ motivated researches on the nickel system thanks to the cheaper price of Ni vs Co. Unfortunately due to instability of Ni^{3+} ions at high temperature, the nickel phase presents the

general global formula: $Li_{1-z}Ni_{1+z}O_2$ ($0.20 < x < 0.01$). The z value is strongly dependent of the synthesis temperature and of the oxygen pressure. The best conditions to have very low z values requires making the reaction at 700°C under pure oxygen. It is necessary to use very reactive lithium sources like Li_2O or LiOH. Li_2CO_3 cannot be used because it requires a too high temperature to be decomposed. From the crystallographic point of view the formula can be written: $(Li_{1-z}Ni^{2+}_{z})[Ni^{2+}_{z}Ni^{3+}_{1-z}]O_2$. In many papers it is considered that there is a Li/Ni exchange between the slab and the interslab space; this is not likely to occur because it would require to have the small Ni^{3+} ions in the lithium layer. The extra-nickel ions are situated in the lithium site and have a dramatic effect on the cycling properties because they prevent the reintercalation of Li^+ ions in their vicinity[84-88]. The almost stoichiometric material which presents a good cyclability (Figure 8) is obtained in very peculiar synthesis conditions which make the synthesis at the industrial scale more difficult than that of LiCoO2. [89,90] Moreover, $LiNiO_2$ is very sensitive to moisture; this requires using very dry atmosphere all along the process from the synthesis to the battery fabrication.

One important point concerns the characterization of the exact stoichiometry on the material. One can use the intensity ratio of the (003)/(104) XRD lines which gives only a tendency. The best ways is to fit the atomic displacement parameter (B_{iso}(Li site)) in the Rietveld analysis of the XRD pattern which is very sensitive to the excess of electronic density carried out by the extra Ni ions.[87] The presence of Ni^{2+} ions in the lithium site has a strong effect on the magnetic properties: there is formation of small ferrimagnetic clusters. The study of the magnetic properties (hysteresis loop) is certainly the most sensitive way to detect Ni^{2+} ions in the Li layer. [91,92] The voltage vs composition curve of a Li//$LiNiO_2$ cell presents a lot of plateaus which indicate the occurrence of structural transitions.[93,94] All the phases were studied by XRD and electron diffraction. On Figure 8, typical electron diffraction patterns, which indicate Li^+/vacancies ordering, are also given with the superstructure cells. [95,96] For all compositions ($x \geq 0.25$) the O3 type oxygen packing is preserved, while when all Li^+ ions have been removed there is formation of the O1 type structure[53] (NiO_2) like CoO_2. Surprisingly the H(1-3) structure was never reported in this system, there is no real explanation about this result. One can assume that the presence of Ni ions in the lithium layer prevents for this phase formation. An interesting point concerns the Li_xNiO_2 ($0.50 < x < 0.75$) solid solution, which exhibits a monoclinic cell with a superstructure due a partial lithium-vacancy ordering.[97] The two end-members correspond to completely ordered structures, while the intermediate solid solution results from the progressive filling of the 2c site, the 2d site remaining unoccupied (Figure 9).

During the lithium deintercalation there is a continuous decrease of the $a_{hex.}$ parameter due to the Ni^{3+} oxidation. The change of the $c_{hex.}$ parameter (Figure 10) is more complicated. In a first step (until x = 0.50) it increases due to the O-O repulsion between adjacent slabs when the screening effect of lithium, directly related to its concentration, decreases. Due to the cation oxidation, the Ni-O bonds become more covalent leading to smaller charges on oxygen anions. This tends to compensate the previous effect and $c_{hex.}$ does not change significantly in the $0.3 < x < 0.5$ range. For lower amount of Li there is formation of the O1 packing (NiO_2) which presents a very small interslab space. As shown in figure 11 the large decrease of the cell volume leads to the particle de-cohesion and the formations of cracks inside the particles. This phenomenon is observed in all layered materials (even in the sodium ones); it leads to a capacity decrease in cycling with $x < 0.3$.

As Ni^{4+} ions are more unstable that the Co^{4+} ones the very deintercalated Li_XNiO_2 phase are very unstable thermally. Therefore, batteries with this material as positive electrode are very unsafe.[98] This lead Moly Energy Company to stop the production of these batteries at the end of the 90's.

Whereas stoichiometric $LiCoO_2$ exhibits a very low irreversible capacity upon cycling, that of $LiNiO_2$ is not negligible and increases considerably with the presence of Ni excess. Nevertheless, even for the most stoichiometric phase this point is not yet fully understood. To try to optimize the $LiNiO_2$ based batteries performances many researches were carried out by a substitution of nickel by various cations. In order to stabilize the ideal layered structure a part of nickel was substituted by various cations: Co, Mn, Al, Fe, Mg, (Co + Mn).

3. 2. 2. $Li_x(Ni,Co)O_2$

The small size of cobalt ions leads to a slab contraction, which destabilizes the large Ni^{2+} ions and stabilizes Ni^{3+}. Therefore, Ni^{2+} ions in the lithium sites are not required for charge compensation. For 20% of substitution ($LiNi_{0.80}Co_{0.20}O_2$) the structure exhibits the ideal layered structure with only Li^+ ions in the interslab space.[18] The cycling curve of this material is shown in Figure 12. The irreversibly is very small and the cell polarization is very low. Structural (XRD) and physical properties characterization (electronic conductivity, thermopower, ^7Li MAS NMR) of the partially deintercalated phases showed that nickel ions are oxidized in the first step during the lithium deintercalation.[99] Cobalt ions are oxidized in the last step leading to electron delocalization.[100] For the intermediate composition $Li_{0.80}Ni_{0.80}Co_{0.20}O_2$ both species are simultaneously oxidized. [101] The electrochemical behavior of this material family is at the origin of intensive studies. [102,103] As cobalt prevents to the presence of Ni^{2+} ions in the lithium layer, this cation is almost always used even

when other substituting cations are considered in lithium nickel oxide. [104] This material[105] is use for a long time in space applications (robots on Mars- NASA). After 9500 cycles with 40% DOD the cell voltage decreased only of 1%.

3. 2. 3. $Li_x(Ni,Mn)O_2$ and $Li_x(Ni,Mn,Co)O_2$

Manganese substitution was studied by Dahn.[106] For the $LiMO_2$ composition, the M cation is at the trivalent state. Mn^{3+} is not stable in front of Ni^{3+}: there is an internal redox reaction leading to formation of Mn^{4+} and Ni^{2+}, a part of Ni^{2+} is in the Li site, leading to a decrease in the cell capacity. In 2001 Ohzuku proposed the $Li(Ni_{1/3}Mn_{1/3}Co_{1/3})O_2$ phase (called NMC333). [107-109]The difference in size between large Ni^{2+} (0.70 Å) cations and small ones (Mn^{4+} (0.54 Å), Co^{3+} (0.53 Å)) and the 1:2 ratio leads to an ordering which was shown by electron diffraction. [110] This ordering allows to accommodate the constraints and then to stabilize this phase with Ni^{2+} in the slabs . The stabilization energy resulting from the ordering prevents from the Ni^{2+}/Li^{+} exchange. Therefore, in this material the first cycle irreversibility is small. This material exhibits very good electrochemical properties and is now intensively used in numerous applications. Due to the presence of Mn^{4+}, Ni^{2+} ions are oxidized in the first step of the deintercalation. Therefore, for a given level of deintercalation, the amount to Ni^{4+} is smaller than in the Li_xNiO_2 system. This improve the thermal stability of the deintercalated material, which is crucial for applications.

The work on NMC 333 was, in the last ten years, extended to all compositions possible in the Li-Mn-Ni-Co-O phase diagram with four goals: (i) to increase the capacity, (ii) to decrease the price, (iii) to increase the safety, (iv) to increase the cycle life. The relative priority between these four parameters depends on the applications. The price being directly related to the material availability, now the tendency is to suppress cobalt and increase the nickel amount for large cells like in EV, which is not relevant from the safety point of view. Nevertheless, researches with other substituting cations are important to understand the reaction mechanism involved in the real cycling of the electrode material and in particular the reactions with the electrolyte a high voltage. To prevent for the parasitic reactions many coating are considered in a very empirical way. Their presence is a key point to optimize real cells.

3. 2. 4. $Li_x(NiAl)O_2$

Ohzuku was the first one to substitute Al for nickel and to show that the thermal stability on the deintercalated phases was significantly increased vs $LiNiO_2$. [111] As aluminum is not active there is a significant decrease of the cell capacity. Depending on the aluminum amount, the very deintercalated phases, which generally induces a capacity lost, cannot be reached. This chemical limitation of the charge prevents for material overcharge and the formation of the unstable deintercalated phases if the amount of aluminum is high enough.

This material family was considered for applications, Ukyo made a very detailed characterization of this material and in particular with Ikuhara showed by very high resolution electron microscopy that there is formation at the particle surface, and also at the grain boundary, of a rocksalt type phase which increases the cell impedance. [112,113]

3. 2. 5. $Li_x(Ni,Fe)O_2$

The effect of substitution of nickel by iron has been also studied. [114] The large size of Fe^{3+} does not destabilize the Ni^{2+} ions present in the slab. The best material, which was obtained, contains 6 % of Ni^{2+} in the lithium layer. [115] Therefore, the cycling curve presents a significant irreversibility (Figure 13a). The redox process involved during the cell charge was followed by Mössbauer spectroscopy. At the very beginning, only nickel is oxidized; then Ni^{3+} and Fe^{3+} are simultaneously oxidized to the tetravalent state. Even, if in principle the iron oxidation is very difficult the large crystal field on the iron site imposed by the neighboring small $Ni^{3+/4+}$ ions, which tends to reduce the Fe-O bond length, makes easier the iron oxidation. As shown in Figure 13b for the fully intercalated phase (x = 0.94) the isomer shift (IS = 0.33 mm/s) is characteristic of Fe^{3+} in octahedral environment. In the case of the strongly deintercalated phase (x = 0.28) three isomer shifts are determined (IS = 0.33, 0.20 and -0.11 mm/s). They are respectively characteristic of Fe^{3+}, $Fe^{(3+\delta)+}$ and Fe^{4+} in octahedral environments. $Fe^{(3+\delta)+}$ indicates an intermediate state due to rapid hopping between Fe^{3+} and Fe^{4+} in comparison to the time constant characteristic of Mössbauer spectroscopy. The understanding of the stabilization of oxidation state is important for the design of safer material in the very deintercalated state.

3. 2. 6. $Li_x(Ni,Co,Mg)O_2$

The change in cell parameters of the electrode materials is one of the main contributions to the fading of lithium-ion batteries. These changes induce constraints within the electrodes; there is a decrease of the cohesion between the particles, which lead to an increase of the cell impedance

and to a capacity loss. In layered oxides upon deintercalation there is a decrease of the a_{hex}. parameter as a result of the M oxidation. In order to limit the cell capacity fading it is necessary to cycle the cell in a limited composition range. Some cationic substitutions were carried out to prevent from too large changes in $c_{hex.}$ parameters. The partial substitution of nickel by magnesium in the $Li(Ni,Co)O_2$ system has been studied in full cells. Figure 14 shows a comparison of the long range capacity of $C//Li(Ni,Co)_2$ and $C//Li(Ni,Co,Mg)O_2$ batteries cycled in the same conditions at 60°C (C rate – 2.7 < V < 4.0 V). [116] In the case of the magnesium substitution, the fading is considerably reduced. The XRD characterization of the pristine material shows that the Mg^{2+} ions are in the Ni,Co sites, while after 500 cycles the main part has migrated to the lithium layer where it acts as a pillar to limit the change in $c_{hex.}$ parameter upon cycling. The Mg^{2+} ions, which are not stabilized by the crystal field, are stable either in octahedra or in tetrahedra; therefore, they can migrate easily from the octahedral site of the MO_2 slab to the octahedral site of the lithium layer. In the case of cobalt and nickel, which are strongly stabilized in octahedral site, this migration is more difficult.

3. 2. 7. Li-rich materials

In this study of the synthesis $Li(Ni_{1-x}Mn_x)O_2$ Dahn discovered that more than 1 Lithium can be present in the material. He showed that if excess lithium is introduced into the transition metal layer a new process occurs during the first charge. [117-118] This was the beginning of the story on overlithiated phases $Li[Li,Ni,Mn,Co]O_2$ which led for the last fifteen years to a considerable research work in the world. [119-123] Thackeray's group made a strong contribution in this field by considering the presence in the $LiMO_2$ and Li_2MnO_3 domains. [124,125] In fact these domains exist only at the very local scale (few octahedra). High resolution electron diffraction shows that the structure is related to the Li_2MnO_3 one with a disorder in the packing of ordered slabs. [126,127] The electrochemical curve exhibits at the first cycle a typical shape shown in Figure 15 when $Li[Li_{0.20}Ni_{0.13}Mn_{0.54}Co_{0.13}]O_2$ is used as starting material. [128] In a first step of the lithium deintercalation Ni and Co are oxidized to the tetravalent state. Then, there is a voltage plateau between 4.5 to 4.7 V where almost all Li^+ ions are removed from the materials. Several models where proposed to explain the oxidation process. Now the community agrees on the following points: (i) part of oxygen is removed from the surface accompanied by a material densification[129,130] that was confirmed by electron microscopy, [131] (ii) in the bulk some O^{2-} ions are partially oxidized[132-134] to $O^{(2-\delta)-}$. During discharge there is reduction of oxygen, nickel and cobalt to the 2-, 2+ and 3+ oxidation state, respectively. The oxygen oxidation in Li_2MnO_3 was suggested by Koyama from First-Principles study. [135] It was shown experimentally

by the Bruce team. [136] Ceder[137] showed for the first time from theoretical calculations that the presence of Li in the metal layer leads to orphaned oxygen orbitals which are not shared with transition metal ions and therefore can be oxidized (Figure 16). This process is reversible during the following cycles. At low voltage, some Mn^{4+} are reduced to Mn^{3+}, which migrate, through a reversible dismutation reaction, to the lithium layer with formation of spinel like nano-domains. This irreversible structure modification leads to a loss of capacity and to a decrease of the cell voltage, which is the main drawback of this material family for applications. Recently, the hypothesis of a contribution of the reversible redox reaction Mn^{4+}/Mn^{7+} was proposed. [138] Even if this hypothesis has not been confirmed experimentally yet, it must be considered. For the homologous lithium rich chromium layered oxides the chromium oxidation to Cr^{6+} was shown by XAS. [139] More detailed characterization have to be carried out to clarify this point.

Many studies were carried out on these materials[140-142] and extended to layered materials with 4d elements and Na-rich layer oxides. [143] For these materials the formation of peroxide pairs is easier than for 3d elements. [144]

3. 3. Thermal stability

The thermal stability of partially deintercalated layered oxides plays a major role on the safety of Li-ion batteries at the charged state. At the discharged state both the negative electrode (graphite) and the positive one ($LiMO_2$) are completely stable. Upon charging there is formation of Li_xC at the negative electrode, which is very reductive vs the liquid electrolyte, and formation of deintercalated Li_xMO_2 at the positive electrode. This material is very oxidizing vs the electrolyte (Fe^{4+}, Ni^{4+} and Co^{4+} are not the standard oxidation state of these elements). Moreover, the deintercalated layered oxides are unstable because of the ionicity of the M-O bond that induces strong repulsions between the oxygen layers when the amount of screening Li^+ ions is not large enough to ensure the structural stability. This behavior is evidenced by the following remark: layered structures are very common in MS_2 chalcogenides whereas, MO_2 layered oxides cannot be obtained by classical solid state chemistry. They were only obtained by electrochemical (or chemical) deintercalation from the homologous lithium phase $LiMO_2$. They are thermally decomposed above 100°C with oxygen loss. This behavior explains why the thermal stability of the cell decreases continuously upon cell charging. From the redox point of view, by increasing the temperature there is tendency to reduce the average transition element oxidation state (oxygen evolution), whereas from the structural point of view there is a tendency to redistribute the transition elements between the slabs and the

interslab sites. The general tendency is to transform the deintercalated layered oxide to spinel and then to rocksalt type phases. It must be kept in mind that the thermal reaction starts from the negative electrode which reacts with the liquid electrolyte, if the temperature of the battery resulting from this reaction is high enough to lead the decomposition of the positive electrode material with oxygen evolution then the runaway occurs.

In the case of the Li_xNiO_2 system, the thermal stability problem was discovered by Dahn. [145] In our lab, the structural modification of the positive electrode material was studied by XRD vs temperature on partially deintercalated materials. Figure 17 shows the change in the XRD patterns obtained from the two starting compositions $Li_{0.50}NiO_2$ and $Li_{0.30}NiO_2$. In both cases the layer structure is transformed into spinel and then to a rocksalt at higher temperature. [146] Because of the increase of the instability when a too large amount of lithium is deintercalated, the decomposition temperature decreases when the lithium content decreases. The thermogravimetric - mass spectroscopy study realized in the same conditions allows following the oxygen departure (Figure 18). From the layered $Li_{0.50}NiO_2$ phase, the $LiNi_2O_4$ spinel phase is formed without oxygen evolution, while in the case of the $Li_{0.30}NiO_2$ phase there is a large oxygen departure at the transition because there no enough lithium in the material to form a stable spinel. In both cases, there is oxygen evolution if the spinel is transformed into rocksalt. This study was extended to the $LiNi_{1-x}Al_xO_2$ system, previously mentioned. As expected the decomposition temperature of deintercalated material was increased. [147] The thermal XRD study of the deintercalated material shows that the spinel formation and the decomposition occur at higher temperature when aluminum is introduced in the structure. [148] One can assume that the stability of aluminum in tetrahedral site delays the spinel formation and its decomposition. A schematic model of the cation migration occurring from layer oxide to spinel is represented in Figure 19. Now the $Li(Ni,Co,Al)O_2$ family (NCA) is used in commercial batteries (EV, HEV, PHEV, space applications).

4. The Na_xMO_2 systems M = 3d cations

Due to the difference in size between Na^+ and M^{3+} cations all $NaMO_2$ elements exhibit the layered structure with the O3 type oxygen packing. The strong ionic character of the Na-O bond vs the Li-O one increases the covalency of the M-O bond, which stabilizes the tetravalent ions. Therefore, contrarily to the lithium homologues the sodium deficient phases Na_xMO_2 can be obtained by high temperature chemistry for V, Mn and Co. They can present either the O3 ($0.9 < x < 1$), P2 ($0.6 < x < 0.8$) or P3 ($0.5 < x < 0.6$) oxygen packings. These limit values can change depending on the

nature of M. The O3 and P2 phases are obtained in the 700°C-900°C range. The P3 phase are not thermally stable, they decompose above 600°C into P2 and metal oxides. Several 3d cations can be mixed in these structures depending on the relative stability of the various oxidation states.

As previously mentioned (Figure 3) the MO_6 octahedra have the same orientation in the O3 and P3 structure, therefore a slab gliding can occur when sodium is deintercalated from O3 $NaMO_2$ with the formation of P3 Na_xMO_2. This reaction is fully reversible; nevertheless, the constraints induced by the gliding limit the long range cycling. The variation of the cell parameter is similar to that on the Li systems (Figure 10). Nevertheless, the decrease of the interslab distance is more important for Na_xMO_2 because at the composition $Na_{\approx 0.3}MO_2$ all materials exhibit a trigonal prismatic environment with a large interslab distance. In all systems, when the amount of Na^+ ions is smaller than ≈0.2-0.3 there is formation of an octahedral environment. "O1" from O3 or P3 and "O2" from P2 starting materials. In fact, in most of the experiments it is difficult to describe really the structure due to the presence of a lot of stacking faults. In most cases, contrarily to the lithium systems, the MO_2 composition is never obtained. On can assume that when the interslab collapses some Na^+ ions remain trapped the structure. In the case of the P2-$Na_x(Fe,Mn)O_2$ systems the formation of the OP4 type structure was mentioned.[149] The formation of a phase with intermediate packing can be related to that of the H1-3(O1-O3) in the Li_xCoO_2 system. [75]

From the electrochemical point of view, the main difference with the lithium materials is the observation of many voltage plateaus due to the strong tendency of Na^+/vacancy ordering for specific compositions. The large size of sodium leads to large repulsive interactions. In the case of the O3 phases the NaO_6 octahedra share only edges with the MO_6 ones; therefore the ordering results only from the Na^+-Na^+ interactions while for materials with trigonal prismatic surrounding the face-sharing between NaO_6 and MO_6 polyhedra leads to more complicated arrangements. Figure 20 shows the cycling curve of a Na battery with P2-$Na_{0.7}CoO_2$[150] as positive electrode material. While there is only one ordered phase ($Li_{0.5}CoO_2$) in the Li_xCoO_2 system, there is a lot of ordered phases in the sodium system. The same behavior is found in the P2-Na_xMnO_2[151], O3-Na_xVO_2[152], O3-Na_xCrO_2[153] and O3-Na_xNiO_2[154] systems. In the case of the vanadium systems the tendency of V^{3+} and V^{4+} ions to make V-V bonds via the overlapping of the t_{2g} orbitals lead to more complicated superstructures with formation of dimers or trimers. The cycling curve obtained for the P2-Na_xVO_2 system[155] and a view of the structure are given in figure 21. On the charge/discharge curve, there is a significant voltage change when the structural transition occurs. The difference in

voltage is directly related to the stabilization energy resulting from the ordering. The shape of the curves with large variation of voltage are not interesting from the application point of view, even if the structural transition are fully reversible. Depending of the size of the particle and of the change in cell parameters at the structural transition, constraints leading to cracks can occur leading to an increase of the cell impedance. Very similar phenomenon occurs when there is structural distortion due to the Jahn-Teller effect of Mn^{3+}. In short, to have a long cycle life, structural transitions must be avoided. For the Li_xCoO_2 and Li_xNiO_2 systems the voltage changes at the ordering/disorder transitions are very small due the low stabilization energy of the ordering. In partially substituted materials, the cycling curves are monotonous. This is evidence that the disordering in the slabs prevent for Li/ vacancy ordering. The same behavior is observed for the Na systems; nevertheless, the ordering is frequently observed for the $Na_{0.5}(L,M)O_2$ composition due to the stronger Na-Na repulsions.

Another difference between lithium and sodium system is the variation on the voltage vs the composition. For the Li//O3-$LiCoO_2$ battery[68] the voltage increases from 4V (x = 0.95) to 4.3 V (x = 0.30) while for Na//O3-$NaCoO_2$ one it increases (Figure 22) from 2.6 V (x = 0.95) to 4.0 V (x = 0.30) This difference in voltage variations[156], independent of the negative electrode, results from the difference of energy of the starting materials. It is easier to deintercalate electrochemically sodium than lithium. It is the same effect, which allows obtaining deintercalated materials by high temperature solid-state chemistry as it was previously explained.

For the O3 type materials the alkali metal ion diffusion requires to go across a tetrahedra; the bottleneck is an oxygen triangle. For the P3 and P2 type materials the intermediate site is a trigonal prism and the bottleneck is an oxygen rectangle. Therefore, the alkali metal diffusivity is easier for the sodium ions in trigonal P2 and P3 structures than for Li of Na in the O3 one. Moreover, the high polarizability of Na^+ ion vs Li^+ make easier the Na^+ diffusion [157] (Figure 23).

4. 1. Na_xCoO_2 and derivatives

Depending on the sodium amount, the O3, O'3, P3 and P2 structural types can be obtained by solid-state chemistry under oxygen[9]. They were used as positive electrode in sodium cells. For all the materials a very good reversibility was obtained. [33] From the O3, O'3 and P3 phases reversible transitions between the three structures were observed. From the P2 phase the structure was maintained in the 4.1-2V range. The electronic properties of deintercalated materials were studied

on sintered pellets which were electrochemically deintercalated to specific compositions. These materials exhibits a very high electronic conductivity in the deintercalated state. [158] This behavior is in agreement with the Goodenough's rule about the electronic delocalization in oxides. [69] The Co-Co distances in the CoO_2 slabs is smaller than the critical distance allowing a t_{2g} orbital overlap through the common edge between CoO_6 octahedra. A very high value of the Seebeck coefficient was also found. It shows that, even if the electron are delocalized, these materials are not "ideal metals". [159] This result was confirmed by Terasaki who found a high value of the Z factor, which characterizes the thermoelectric materials. [160] In 2003, Takada reported the supraconductivity at 5 K of hydrated Na_xCoO_2. [161] These two discoveries stimulated many researches from physicists on the structure and physical properties of these materials. Single crystals were made by floating zone at high temperature; in these conditions, it is difficult to know exactly their compositions. In order to really determine the true phase diagram of the P2-Na_xCoO_2 system we made an electrochemical in situ XRD experiment during the charge of the cell. It shown the occurrence of many structural transitions due to Na^+/Vacancy ordering[150] (superstructure or modulation) (Figure 24).

Among the various substitutions, which were made from the $NaCoO_2$ phase, one has to mention the P2-$Na_{2/3}Co_{1-y}Mn_yO_2$ system which was explored in details by Yamada. [162] The relative effect of the cations, depending on the y values, on the cell voltage was shown. For the P2-$Na_{2/3}Co_{2/3}Mn_{1/3}O_2$ phase magnetic measurements and ESR analyses of the pristine material confirm the expected presence of Co^{3+} and Mn^{4+}ions. [163] Contrarily, to the homologous P2-$Na_xNi_{2/3}Mn_{1/3}O_2$ phase studied by Dahn, the classical ordering is not observed in the slab for the 2/3 - 1/3 cationic ratio of the transition metals. [164] The Co^{3+} and Mn^{4+} ions have very similar radii; this shows that the ordering results from the difference in size and not from the charge of the cations which can contribute in the second order. The discharge curve of the battery with the P2-$Na_{2/3}Co_{2/3}Mn_{1/3}O_2$ phase is compared to the P2-Na_xCoO_2 one on Figure 25. Both curves present a voltage drop at the composition x = 0.5 due to Na^+/vacancy ordering. When sodium is intercalated there is large decrease of the cell voltage due to low voltage of the $Mn^{4+/3+}$ couple. In fact, an XAS study has shown that a part on Co^{3+} is reduced to Co^{2+} at low voltage. [165]

In the case of the O3-$NaCo_{1/2}Fe_{1/2}O_2$ phase good electrochemical performance were obtained. Micro-sized material exhibits very good behavior at high rate. [166]

4. 2. Na_xMnO_2 and derivatives

In the Na_xMnO_2 system, the structural types O'3-$NaMnO_2$ and P2-$Na_{\approx 0.70}MnO_2$ were obtained, for the first time, by solid state chemistry under oxygen by Fouassier. [50] O'3-$NaMnO_2$ crystalizes in the monoclinic system (C2/m) thanks to the Jahn-Teller effect of Mn^{3+}. During the Na deintercalation there is oxidation of Mn^{3+} to Mn^{4+} which is not a Jahn-Teller active ion. A very detailed study of the "$Na_{2/3}MnO_2$" phase was made by Stoyanova who confirmed the presence of Mn vacancies by ESR and magnetic measurements.[167] Both O3 and P2 phases were characterized from the electrochemical point of view. [34] Ceder showed from the O'3-$NaMnO_2$ phase a significant difference between the shapes of the charge and discharge curves which indicates a reversible hysteresis phenomena.[168] This result was recently confirmed by a very detailed characterization which shows the existence of several ordered phase.[169] The simultaneous presence of Jahn-Teller distorted $Mn^{3+}O_6$ octahedra and to non-distorted $Mn^{4+}O_6$ ones induces local constraints in the material, which can be minimized by cation charge ordering. This can lead to many superstructures where the Na/vacancy ordering occurs with the charge ordering. This was shown for the first time for the $Na_{5/8}MnO_2$ composition.[170] The "super charge separation" associated to Na^+ ordering was observed for $Na_{1/3}MnO_2$ and $Na_{1/2}MnO_2$ compositions.[169] P'2-$Na_{0.70}MnO_2$, which contains 30 % of Mn^{4+} ions, crystalizes in the orthorhombic system (Cmcm) while the P2 "$Na_{0.70}MnO_2$" which is obtained under 4 bars of oxygen crystalizes in the hexagonal ($P6_3/mmc$). It contains an excess of oxygen. Its chemical formula is $Na_{0.70}MnO_{2+y}$ ($0.05 < y < 0.12$). In fact, the structural formula is $Na_{1.4/(2+Y))}MnO_{2/(2+y)}O_2$, which indicates the presence of manganese vacancies in the slab. In this oxidized material, the amount of Mn^{3+} is reduced leading to the disappearance of the cooperative Jahn-Teller effect.

The Komaba's group, who succeeded to synthesize for the first time the ideal material without any manganese vacancy, clarified the effect of the presence of Mn vacancies in the P2 phase on the electrochemical behavior. [171] They shows that this material, with Jahn-Teller distortion, exhibits a larger reversible capacity and a reduced fading upon cycling than that of the oxidized phase with Mn vacancies. Nevertheless, there is no clear explanation of what is going on.

Among the various studies reported on substituted materials, the $Na_x(Fe,Mn)O_2$ system is particularly interesting either for the application point of view and for the scientific one.[172,173] Several Fe/Mn ratio were considered. [174-183] Sodium batteries with the O3, P3 and P2 phases were cycled in various voltage range. The best results were obtained for the P2-$Na_x(Fe_{0.5}Mn_{0.5})O_2$ phase (200 mAh/g) at the first cycle. On cycling there is a decrease of the capacity, principally when the upper limit of voltage is higher than 4.0 V. This phenomenon, observed in all systems, is related to

the slab gliding which occurs when a too large amount of sodium is deintercalated from the interslab space. Mössbauer spectroscopy shows that iron is involved in the redox process. Figure 26 represents the Mössbauer spectra of materials obtained (ex situ) by intercalation and deintercalation in the P2-$Na_x(Fe_{0.5}Mn_{0.5})O_2$ phase. For $x \geq 0.5$ only Fe^{3+} is observed, as expected. For x=1, all Mn^{4+} ions are reduced to Mn^{3+}, there is a broadening of the pattern characteristic of a distribution of quadrupolar effects resulting from the local distortions of $Mn^{3+}O_6$ octahedra (Jahn-Teller effect of Mn^{3+}). For $x < 0.5$, there is a change in the isomer shifts, characteristic of the oxidation of Fe^{3+} in Fe^{4+} and $Fe^{(3+z)+}$. $Fe^{(3+z)+}$ corresponds to an intermediate oxidation state when one electron is exchanged between Fe^{3+} and Fe^{4+} ions. [184] Depending on the Fe/Mn ratio the redox domain of the Fe^{3+}/Fe^{4+} and Mn^{3+}/Mn^{4+} couples overlap or not. If there is an overlapping there is a continuous increase of the voltage in charge while, if there is no overlapping there is a voltage gap. In this case, at the exact composition when there is only Mn^{4+} and Fe^{3+}, there is strong decrease of the electronic conductivity (larger polarization) of the electrode. [185

4. 3. $Na_x(Li,Mn)O_2$ and $Na_x(Mg,Mn)O_2$

Yabuuchi and Komaba in their very first study on the P2-$Na(Li,Mn)O_2$ system suggested the oxygen oxidation to explain the electrochemical behavior. [186] The oxygen oxidation was confirmed by DFT calculations[187] and extended to the P3-type structure. [188,189] The P2-type $Na_{0.72}[Li_{0.24}Mn_{0.76}]O_2$ phase, where all manganese ions are tetravalent exhibits a high initial charge capacity of 210 mAh/g (0.72 Na) based on a pure anionic redox reaction. The P2 structure can be maintained upon cycling. [190]

By analogy to the lithium rich materials, sodium layered phase with Mg and Li in the MO_2 slabs were considered. [191] Bruce and coworkers have shown that Na can be deintercalated from the $Na_{2/3}(Mg_{0.28}Mn_{0.72})O_2$, which contains a small amount of Mn^{3+} ions. [192] This behavior is very similar to that of the lithium-rich materials. The oxygen surrounding Mg^{2+} ions, in the MO_2 slabs, exhibits orphaned 2p orbitals, allowing oxygen oxidation.

4. 4. Na_xNiO_2 and derivatives

Due to the instability of Ni^{4+} the partially deintercalated phases were never reported by high temperature solid state chemistry. Like $NaMnO_2$, $NaNiO_2$ crystallize in the C2/m space group (LS Ni^{3+} is a Jahn-Teller ion). [51] There is only a few studies of their electrochemical properties. [33,193-195] The charge/ discharge curve (Figure 27) of a $Na//Na_xNiO_2$ battery presents several phase transitions

corresponding to peculiar values of x (1/3, 2/5, ½, 2/3). For all of them, the cell parameters where determined. [33,194] For Na_xNiO_2 (x = 2/5, ½, 2/3) there is evidence of superstructures. The cell parameters of the supercell were determined, but the detailed structures have never been solved. [195] The substitution of nickel by cobalt ($NaNi_{0.6}Co_{0.4}O_2$) suppresses the sodium/vacancy ordering in the deintercalated material. Upon deintercalation the O3↔O'3 and O'3↔P'3 transitions occur successively. The magnetic and electronic conductivity studies on the deintercalated material shows that nickel is oxidized before cobalt. The very high electronic conductivity of the P'3 phase (Co^{3+}/Co^{4+}) and the presence of the trigonal prismatic environment lead to a very small polarization of the cell. [35]

The partial substitution of Ni by Mn allows to get rid of the presence of the Jahn-Teller Ni^{3+} ions. The internal redox reaction between Ni^{3+} and Mn^{3+} leads to Ni^{2+} and Mn^{4+}. In 1999, Paulsen and Dahn synthesized the P2-$Na_{2/3}(Ni_{1/3}Mn_{2/3})O_2$ phase and then opened the way to the whole material family.[196] In this phase, there is a honeycomb ordering between the large Ni^{2+} ions and the small Mn^{4+} ones. These materials were used by as precursor to obtain metastable lithium phases, which were carefully studied. [197] The partial substitution of nickel by cobalt prevents for the existence of the superlattice and leads to the presence of stacking faults in the lithium exchanged material. [198] Then the P2-$Na_{2/3}(Ni_{1/3}Mn_{2/3})O_2$ and O3-$Na(Ni_{1/2}Mn_{1/2})O_2$ materials were really considered for practical intercalation electrodes. In both systems, Ni^{4+} are formed only in the second part of the deintercalation process, which is key point to increase the battery safety. From the P2 phase at 4.2 V vs Na/Na^+ there is formation of the O2 phase by slab gliding. [199] Even if the structural transition is completely reversible from the structural point of view, there is an important capacity decrease during long range cycling. If the upper limited voltage is limited to 4.1 V the fading is significantly reduced. [200] The capacity lost on the 4.2 V plateau has been recently related to oxygen evolution. [201] Similar results were obtained by deintercalation / intercalation from the O3-$Na(Ni_{1/2}Mn_{1/2})O_2$ phase. The reversible structural O3 ↔ P3 transition occurs, followed by a voltage plateau at 4.2V, where the classical collapse of the interslab distance occurs. [202-204]

The O3-$Na(Ni_{0.6}Fe_{0.4})O_2$ phase studied by the Yamada group shown that to metal charge transfer, which suppresses local distortion of the Jahn-Teller Ni^{3+} ion, can also contribute to the improved cycle stability. [205]

4. 5. $NaTiO_2$ and derivatives

Sodium deintercalation from $NaTiO_2$ was reported more than 30 years ago. An irreversible Ti migration was observed when more than 0.3 Na were deintercalated due to the non-crystal field stabilization of Ti^{4+} in octahedral site. [206] The Huang's group synthesized the P2-$Na_{0.66}(Li_{0.22}Ti_{0.78})O_2$ phase and use it as negative electrode. In this experiment, the Ti^{4+}/Ti^{3+} redox couple is involved. 0.34 sodium can be reversible intercalated at low voltage between 1.0 V and 0.5 V without any change in cell parameters, leading to a zero-strain-material. [207] This original approach was extended to the P2-$Na_{0.66}(Cr_{0.6}Ti_{0.4})O_2$ phase. This material can be used either as a positive electrode (Cr^{3+}/Cr^{4+} redox couple) or as a negative electrode (Ti^{4+}/Ti^{3+} redox couple) leading to a symmetric battery able to be cycled at high rate. [208]

4. 6. Poly-substituted materials

From the previously presented materials, many experiments were made to try to optimize the material performances. The main goal was to prevent the capacity fading at high voltage. Up to four transitions elements were used among (Co,Ni, Mn, Fe, Cu, Mg, Ti, Ca-, Zn).[209-219] Whatever the starting material (P2 or O3 type), in all cases there is at around 4.2 V vs Na/Na^+ a phase transition with formation of octahedral environments for the remaining sodium ions associated to the large decrease of the interslab distance which induces cracks in the particles. This leads to a rapid decrease of the reversible capacity. When copper is introduced in the lattice (10% of the transition elements), there is stability of the cycling capacity. It was assumed that the presence of inactive Cu^{2+} Jahn-Teller distorted (CuO_6) octahedra stabilizes the distorted P'2 structure and limits the structural constraints. [220] Some promising experiments were made by incorporation of inactive ions (Mg[221], Ca[222]) with large size which can move to the Na layer and then acts as a pillar to prevent the slab gliding at high voltage and limit the collapse of interslab distance.

5. Conclusion

Forty years after the John Goodenough's discovery, the layered oxides are always the main used positive electrode materials in lithium-ion batteries. A huge number of compositions were considered to understand the mechanism involved during the cycling and to try stabilizing the structure in a large lithium (sodium) composition domain. The safety problems have been significantly reduced by cationic substitution. Now, the new characterization techniques allow to

analyse the material at very small scale. The tendency is to add very small amount of some elements and to make specific coatings.

Cobalt, is used (at least partially) for small batteries, which deliver the highest energy density (Wh/Kg or Wh/l). For a few years researches on positive electrode materials are focused on Ni Rich for EV, HEV, PHEV thanks to their very high energy density. The problem of their low thermal stability must be solved. Even, if all compositions seem to have already been tested, one can expect new improvements in the future.

Acknowledgements

The authors thanks all their students, postdocs and coworkers (M. Ménétrier, L. Croguennec, F. Weill, A. Wattiaux and C. Denage) for their contribution to the study of layered oxides. CNRS, CNES, Saft, Umicore, Toyota and Région Nouvelle Aquitaine are acknowledged for financial supports.

Conflict of Interest

The authors declare no conflict of interest.

References

1 M.S. Whittingham, *Science*, **1976**, *192*, 1126.

2 2 S. Witthingham, *J.Elect. Chem. Soc.*, **1976**,*123*, 315.

3 3 D.Win, J. Shemilt and B. Steele, *Mat.Res. Bull.,* **1976**, *11*, 559.

4 D. Murphy and F. TrumBore, J*. Crystal Growth.*, **1977**, *39*, 1185.

5 M. Armand and P. Touzain, *Mater. Sc. and Engineer.*, **1977**, *31*, 319.

6 W. Johnson, R. Heikes and D. Sestrich, *J. Phys. Chem. Solids*, **1958**, 7, 1

7 K. Mizushima, P.C. Jones, P.J. Wiseman and J.B. Goodenough, *Mater. Res. Bull.,* **1980**, 15, 783.

8 C. Delmas, J.J. Braconnier, C. Fouassier and P. Hagenmuller, *Solid State Ionics*, **1981** *3/4*, 165.

9 C. Fouassier, G. Matejka, J-M. Reau, and P. Hagenmuller, *J Sol. State Chem.*, **1973**, *6*, 532.

10 A. Yoshino et al., USP4, 668,595 and JP1989293, filing date (priority) May 10, 1985 (Basic patent of the LIB. Certain crystalline carbon).

11 J. Dahn, U. Von Sacken, and C. Michal, *Solid State IonIcs*, **1990**, *44*, 87.

12 W. Li, J. Riemers and J. Dahn, *Phys Rev. B Cond. Mat. & Mat. Phys.*, **1992**, *45*, 3236.

13 T. Ohzuku, A. Ueda and M. Nagayama, *J. Electrochem. Soc.,* **1993**, *140*, 1862

14 T. Ohzuku, A. Ueda, M. Nagayama, Y. Iwakoshi, and H. Komori, *Electrochem. Acta,* **1993**, *38*, 1159

15 M. Broussely, F. Perton, P. Biensan, J.M.Bodet, J. Labat, A. Lecerf, C.Delmas, A. Rougier and J.P. Peres, *J. of Power Sources,* **1995,** *54***,** 109.

16 A. Rougier, P. Gravereau and C. Delmas, *J. Electrochem. Soc*., **1996**, *143*, 1168.

17 J.P. Peres C. Delmas, A. Rougier, M. Broussely, F. Perton, P. Biensan and P. Willmann, *J. Phys. Chem Solids,* **1996**, *57*, 1057.

18 C. Delmas and I. Saadoune, *Solid State Ionics*, **1992**, *53-56*, 370.

19 E. Rossen, C. Jones and J. Dahn, Solid State IonIcs*,* **1992**, *57*, 311.

20 T. Ohzuku and M. Yoshinari, Chemistry letters, **2001**, *30*, 744.

21 J. Reimers, E. Rossen, C. Jones and J. Dahn, *Solid State IonIcs,* **1993**, *61*, 335.

22 T. Ohzuku, A. Ueda and M. Kouguchi, *J. Electrochem. Soc.,* **1995**, *142*, 4033.

23 T. Ohzuku, T. Yanagawa and M. Kouguchi, A. Ueda, *J. Power Sources*, **1997**, *68*, 131.

24 T. Ohzuku, K. Nakura and T. Aoki, *Electrochem. Acta*, **1999**, *45*, 151.

25 N. Yabuuchi and T. Ohzuku, *J. Power Sources* **2003**, *119*, 171.

26 N. Yabuuchi and T. Ohzuku, *J. Power Sources* **2005**, *146*, 636.

27 S. Madhavi, G. Subba Rao, B. Chowdari and S. Li, *J. Power Sources,* **2001**, *93*, 156.

28 M. Broussely, Ph. Blanchard, Ph, Biensan, J.P. Planchat, K. Nechev and R. Staniewicz, *J. Power Sources,* **2003**, *119*, 859.

29 T. Nonaka, C. Okuda, Y. Seno, H. Nakano, K. Koumoto and Y. Ukyo, *J. Power Sources*, 2006, 162, 1329.

30 T. Sasaki, T. Nonaka, H. Oka, C. Okuda, Y. Itou, Y. Takeuchi, Y. Ukyo, K. Tatsumi and S. Muto, *J. Electrochem. Soc.,* **2009**, *156*, A289.

31 S. Zheng, R. Huang, Y. Makimura, Y. Ukyo, C. Fisher, T. Hirayama and Y. Ikuhara, *J. Electrochem. Soc.*, **2011**, *158*, A 357.

32 A. Maazaz, C. Delmas and P. Hagenmuller, *J. of Incl. Phenomena,* **1983**, *1*, 45.

33 J-J. Braconnier, C. Delmas and P. Hagenmuller, *Mat. Res. Bull.,* **1982**, *17*, 993.

34 A. Mendiboure, C. Delmas and P. Hagenmuller, *Mat. Res. Bull.,* **1984,** *19*, 1383.

35 I. Saadoune , A. Maazaz, M. Menetrier and C. Delmas, *J. Solid State Chem.,* **1996**, *122*, 111.

36 J.M. Tarascon and G.W. Hull, *Solid State Ionics*, **1986**, *22*, 85.

37 K. Kubota, N. Yabuuchi , H. Yoshida , M. Dahbi, and S., Komaba, *MRS Bull.,* **2014**, *39*, 416.

38 S. Komaba, T. Nakayama, A. Ogata, T. Shimizu, C. Takei, S.Takada, A. Hokura, I. Nakai, I. *ECS Trans.,* **2009**, *16*, 43.

39 Z. Yang, J. Zhang, M. C. W. Kintner-Meyer, X. Lu, D. Choi, J. P. Lemmon and J. Liu, *Chem. Rev.,* **2011**, *111*, 3577.

40 B. L. Ellis and L. F. Nazar, Cur. *Opinion Sol. State and Material Sc.,* **2012**. *16*, 168.

41 S.-W. Kim, D-H. Seo, X. Ma , G. Ceder and K. Kang, *Adv. Energy Mater.* **2012**, *2*, 710.

42 V. Palomares, P. Serras, I Villaluenga, K.B. Hueso J. Carreetero- Gonzalez and T. Rojo, *Energy Environ Sc.*, **2012**, *5*, 5884.

43 H. Kim, H. Kim, Z. Ding, M. H. Lee, K. Lim,G. Yoon , and K. Kang, *Adv. Energy Mater.* **2016**, *6*, 1600943.

44 M.-A. Muñoz-Marquez, D. Saurel, J. L. Gómez-Camer, M. Casas-Cabanas, E. Castillo-Martínez, and T. Rojo, *Adv., Energy Mater.,* **2017**, 1700463.

45 J.-Y. Hwang, S.-T. Myung and Y.-K. Sun, *Chem. Soc. Rev.*, **2017**, *46*, 3529

46 Y-K Sun. h, S-T. Myung, B-C. Park, J. Prakas, I Belharouak and K. Amine, *Nat. Mater.,* **2009**, *8*, 320.

47 Y-K. Sun, Z. Chen, H-J. Noh, D-J. Lee, H-G. J. Y. Ren, S. Wang,

52 G. Amatucci, J.M. Tarascon et L.C. Klein, *J. Electrochem. Soc.,* **1996***,143*, 1114.C-S. Yoon, S-T. Myung and K. Amine, *Nat. Mater.,* **2012**, *11*, 942.

48 C. Yoon, K-J. Park, U-H. Kim, H-H. Ryu and Y-K. Sun, *Chem. Mater.,* **2017**, *29*, 10436.

49 C. Delmas, C. Fouassier and P. Hagenmuller, *Physica*, **1980,** *99B*, 81.

50 J.P. Parant, R. Olazcuaga, M. Devalette, C. Fouassier and P. Hagenmuller, *J. Solid State Chem.*, **1971**, *3*, 1.

51 L.D. Dyer, B.S. Borei and J.P. Smith, *J. Amer Chem. Soc.,* **1954**, *76*, 1499.

52 G. Amatucci, J.M. Tarascon and L.C. Klein, *J. Electrochem. Soc.,* **1996***,143*, 1114.

53 L. Croguennec, C. Pouillerie, C. Delmas, *Solid State. Ionics,* **2000**, *135*, 259.

54 F. Capitaine, P. Gravereau and C. Delmas, *Solid State Ionics,* **1996**, *89*, 197.

55 A.R. Armstrong and P.G. Bruce, *Nature,* **1996***, 381*, 499.

56 C. Delmas, J.J. Braconnier, and P. Hagenmuller, *Mat. Res. Bull.,* **1982***, 17*, 117.

57 D. Carlier, I. Saadoune, L. Croguennec, M. Menetrier, E. Suard, C. Delmas, *Solid. State. Ionics,* **2001**, *144*, 263.

58 J. Paulsen, C. Thomas, J. Dahn, *J. Electrochem. Soc.,* **2000**, *174*, 861.

59 Z. Lu and J.R. Dahn, *J. Electrochem. Soc., **2001***, *148*, A1225.

60 R. Balsys and R. Lindsay, *Solid. State Ionics,* **1994**, *69*, 69.

61 R. Berthelot, M. Pollet, D. Carlier and C. Delmas, *Inorg. Chem.,* **2011**, *50*, 2420.

62 R. Berthelot D. Carlier, M. Pollet, J.-P. Doumerc and C. Delmas, *Electrochem. Solid State Lett.,* **2009**, *2(11)*, A207.

63 S. Komaba, N. Yabuuchi, Y. Kawamoto, *Chem. Letters,* **2009**, 3*8(10)*, 954.

64 L. Picciotto, M. Thackeray, W. David, P. Bruce and J. Goodenough, *Mat. Res. Bull.,* **1984**, *19*, 1497.

65 M. Tabuchi, K. Ado, H. Kobayashi, H. Kageyama, C. Masquelier, A. Kondo and R. Kanno, *J. Electrochem. Soc*., **1998**, *145*, L49.

66 J. M. Paulsen, C. L. Thomas, and J. R. Dahn, *J. Electrochemical Soc.,* **1999**, *146,* 3560.

67 A. Manthiram, Nature. Com., **2020** doi.org/10.1038/s41467-020-15355-0.

68 M. Duffiet, M. Blangero, P-E. Cabelguen, C. Delmas and Dany Carlier, *J. Phys. Chem. Lett.,* **2018**, *9*, 5334.

69 D. Rogers, R. Arnott, A. Wold and J. Goodenough, *J. Phys. Chem. Solids,* **1963**, *24*, 374.

70 M. Menetrier, I. Saadoune, S. Levasseur and C. Delmas, *J. Mater. Chem.,* **1999**, *9*, 1135.

71 A. Van der Ven, M. Aydinol, G. Ceder, G. Kresse and J. Hafner, *Phys. Rev. B*, **1998**, *58(6)*, 2975.

72 J.N. Reimers and J.R. Dahn, *J. Electrochem Soc.*, **1992**, *139*, 2019.

73 T. Ohzuku, A. Ueda, *J. Electrochem Soc*., **1994**, *141*, 2972.

74 Y. Shao-Horn, S. Levasseur, F. Weill and C. Delmas, *J. Electrochem Soc.*, **2003**, *150*, A366.

75 A. Van der Ven, M.K. Aydinol and G. Ceder, *J. Electrochem. Soc*., **1998**, *145(8)* 2149.

76 C. Zhaohui, L. Zonghua, J.R. Dahn, *J. Electrochem. Soc.,* **2002**, *149(12)* A1604.

77 N. Daumas and A.Herold, *C. R. Acad. Sc*i. Paris, **1969**, *268*, 373.

78 M. Carewska, S. Scaccia, F. Croce, S. Arumugam, Y. Wang, S. Greenbaum, S. *Solid State Ionics*, **1997**, *93*, 227.

79 S. Levasseur, M. Menetrier, E. Suard, and C. Delmas, *Solid State Ionics*, **2000**, *128*, 11.

80 S. Levasseur, M. Menetrier, Y. Shao-Horn, L; Gautier, A. Audemer, G. Demazeau, A. Largeteau and C. Delmas, *Chem. Mater*., **2003**, *15*, 348.

81 M. Menetrier, D. Carlier, M. Blangero and C. Delmas, *Electrochem. and Solid-State Letters,* **2008**, *11* , A179.

82 Y. Koyama, H. Arai, I. Tanaka, Y. Uchimoto, and Z. Ogumi, *Chem. Mater.*, **2012,** *24*, 3886.

83 D. Carlier, J.-H. Cheng, C .J. Pan, M. Menetrier, C. Delmas, and B-J. Hwang, *J. Phys. Chem. C*, **2013**, *117*, 26493.

84 J. Morales, C. Perez-Vicente and J.L. Tirado, *Mater. Res; Bull.*, **1990**, *25*, 623.

85 W. Li, J.N. Reimers and J.R. Dahn, *Phys. Rev.*, **1992**, *B46*, 3236.

86 T. Ohzuku, A. Ueda and M. Nagayama, *J. Electrochem. Soc*., **1993**, *140*, 1862.

87 A. Rougier, P. Gravereau and C. Delmas, *J. Electrochem. Soc*., **1996**, *143*, 1168.

88 J.P. Peres C. Delmas, A. Rougier, M. Broussely, F. Perton, P. Biensan and P. Willmann, *J. Phys. Chem Solids,* **1996**, *57*, 1057.

89 M. Broussely, F. Perton, P. Biensan, J.M.Bodet, J. Labat, A. Lecerf, C.Delmas, A. Rougier and J-P. Peres, *J. Power Sources,* **1995**, *54*, *109*.

90 C. Delmas, J.P. Peres, A. Rougier, A. Demourgues, F. Weill, A. Chadwick, M. Broussely, F. Perton, Ph. Biensan, P. Willmann, *J. Power Sources,* **1997**, *68*, 120.

91 J. Reimers, J. Dahn, J. Greedan, C. Stager, G. Liu, I. Davidson and U. Von Sacken, *J. Solid State Chem.*, **1993**, *102*, 542

92 A. Rougier, C. Delmas and G. Chouteau, *J. Phys. Chem. Solids*, **1996**, *57*, 1101.

93 W. Li, J.N. Reimers and J.R. Dahn, *Solid State Ionics*, **1993**, *67*, 123.

94 H. Arai, S. Okada, H. Ohtsuka, M.Ichimura, and J. Yamaki, *Solid State Ionics,* **1995**, *80*, 261.

95 C. Delmas, J.P. Peres, A. Rougier, A. Demourgues, F. Weill, A. Chadwick, M. Broussely, F. Perton, Ph. Biensan and P. Willman, *J. Power Sources*, **1997**, *68*, 120.

96 J.-P. Peres, *PhD thesis,* University Bordeaux, **1996**.

97 J-P. Peres, F. Weill and C. Delmas, *Solid State Ionics*, **1999**, *116*, 19.

98 J. Dahn, E. Fuller, M. Obrovac, U. Sacken, *Solid State Ionics*, *1994*, *69*, 265.

99 M. Menetrier, A. Rougier and C. Delmas, *Solid State Com.,* **1994**, *90*, 439.

100 I. Saadoune, M. Menetrier and C.Delmas, *J Mater. Chem.,* **1997**, *7(12)*, 2505.

101 D. Carlier, M. Menetrier and C. Delmas, *J. Mater. Chem*., **2001**, *11*, 594.

102 R. Alcantara, P. Lavela, J. L. Tirado, R. Stoyanova and E. Zhecheva, *J. Electrochem. Soc.*, **1998**, *145*, 730.

103 J. Cho, G. Kim and H. S. Lim, *J. Electrochem. Soc.,* **1999**, *146*, 3571.

104 T. Ohzuku, K. Nakura, T. Aoki, *Electrochimica Acta*, **1999**, *45*,151.

105 C. Delmas, I. Saadoune and A. Rougier, *J. Power Sources,* **1993**, 43-44, 595.

106 E. Rossen, C. Jones, and J. Dahn, *Solid State Ionics*, **1992**, *57*, 311.

107 T. Ohzuku and Y. Makimura, *Chem Letters*, **2001**, *30*, 642.

108 Y. Koyama, I. Tanaka, H. Adachi, Y. Makimura, T. Ohzuku, *J. Power Sources*, **2003**, *19*, 644.

109 N. Yabuuchi, Y. Makimura, T. Ohzuku, *J. Electrochem. Soc*., **2007**, *154*, A314.

110 N. Yabuuchi, Y. Koyama, N. Nakayama and T. Ohzuku, *J. Electrochem. Soc*., **2005**, *152*, A1434.

111 T. Ohzuku, T. Yanagawa, M. Kouguchi and A. Ueda, *J. Power Sources*, **1997**, *68*, 131.

112 S. Zheng, R. Huang, Y. Makimura, Y. Ukyo, F. Craig, T. Hirayama and Y. Ikuhara, *J. Electrochem. Soc.*, **2011**, *158*, A362.

113 Y. Makimura,S. Zheng, Y. Ikuhara, Y. Ukyo, *J. Electrochem. Soc.*, **2012**, *159*, A1070.

114 J.N. Reimers, E. Rossen, C.D. Jones and J.R. Dahn, *Solid State ionics*, **1993**, 61(4), 335.

115 C. Delmas, G. Prado, A. Rougier, E. Suard, L. Fournes. *Solid State Ionics,* **2000**, *135*, 71.

116 C. Pouillerie, L. Croguennec et C. Delmas, *Solid State Ionics,* **2000**, *132*, 15.

117 Z. Lu, L.Y. Beaulieu, R.A. Donaberger, C.L Thomas and J.R. Dahn, *J. Electrochem. Soc.,* **2002**, *149(6*), A778.

118 Z. Lu and J.R. Dahn, J. Electrochem. Soc., **2002,** *149(7)*, A815.

119 J.S. Kim, C. Johnson, J. Vaughey , M. Thackeray, S. Hackney, W. Yoon and C. Grey, *Chem. Mat.*, **2004**, *16*, 1996.

120 M. Thackeray, S.H. Kang, C. Johnson, J. Vaughey , R. Benedek and S. Hackney, J. Mater. Chem., **2007**, *17*, 3112.

121 N. Tran, L. Croguennec, M. Menetrier, F. Weill, P. Biensan, C. Jordy and C. Delmas, *Chem. Mater.*, **2008**, *20*, 4815.

122 K. Jarvis, Z. Deng, L. Allard, A. Manthiram and P. Ferreira, *Chem. Mater.*, ,**2011** ,*23*, 3614.

123 J.H. Hong, H.D. Lim, M. Lee, S.W. Kim, H. Kim, S.T. Oh, G.C. Chung and K. Kang, *Chem.Mat.*, **2012**, 24, 2692.

124 C. Johnson, N. Li, C Lefief and M. Thackeray, Electrochem. Com.

125 J. Croy, S. Kim, M Balasubramanian, K. Gallager, S6H. Kang and M. Thackeray, *J. Electrochem. Soc.,* **2012**, *159*, A790, **2007**, *9*, 787.

126 K. Jarvis, Z. Deng, L. Allard, A. Manthiram and P. Ferreira, *Chem. Mater.* **2011**, *23*, 3614.

127 M. Gu, I Belharouak, D. wong, K. Amine, S. Theyuthasan,D. Baer, J-G Zhang, N. Browing, J Liu and C. Wang, *Chem. Mater.* **2013**, *25*, 2319.

128 H. Koga, L. Croguennec, P. Mannessiez, M. Ménétrier, F. Weill, L. Bourgeois, M. Duttine, E. Suard, and C. Delmas, *J.of Physical Chemistry* C, **2012**, *116*, 13497.

129 R. Armstrong, M. Holzapfel, P. Novak, C. Johnson, S-H. Kang, M. Thackeray and P. Bruce, *J. Am. Chem. Soc.*, **2006**, *128*, 8694.

130 N. Tran, L. Croguennec, M. Menetrier, F. Weill, Ph. Biensan, C. Jordy, and C. Delmas, *Chem. Mater.* **2008,** *20,* 4815.

131 A. Boulineau, L. Simonin, J.-F. Colin, C. Bourbon and S. Patoux, *Nano Lett.,* **2013**, *13*, 3857.

132 A. Ito, Y. Sato, T. Sanada, M. Hatano, H. Horie and Y. Ohsawa, *J. Power Sources*, **2011**, *196*, 6828.

133 H. Koga, L. Croguennec, M. Menetrier, P. Mannessiez., F. Weill, C. Delmas, *J. Power Sources*, **2013**, *236*, 250.

134 H. Koga, L. Croguennec, M. Menetrier, P. Mannessiez, F. Weill, C. Delmas and S. Belin, *J. Phys. Chem. C*, **2014**, *118*, 5700.

135 Y. Koyama, I. Takana, M. Nagao and R. Kanno. *J. Power Sources*, **2009**, *189*, 708.

136 K. Luo, M. Roberts1, R. Hao, N. Guerrini, D. Pickup, Y-S. Liu, K. Edström, Ji. Guo, A. Chadwick L. Duda, and P. Bruce, *Nat. Chem.,* **2016**, *8*, 684.

137 D-H. Seo, J. Lee, A. Urban, R. Malik, S. Kang and G. Ceder, *Nat. Chem.,* **2016**, *8*, 692.

138 M. Radin, J. Vinckeviciute, R. Seshadri and A Van der Ven, *Nat. Energy,* **2019** *4*, 636.

139 B. Ammunsen, J. Paulsen, I. Davidson, R-S. Liu, C-H. Shen, J-M. Chen, L-Y. Jang and J-F Lee, *J. Electrochem.* Soc., 2002, 149, A431.

140 M. Okubo and A. Yamada, *ACS Appl. Mater. Inter.*, **2017**, *9*, 36463.

141 M. Sathiya, A. Abakumov, D. Foix, G. Rousse, K. Ramaesha, M. Saubagnere, M-L. Doublet, H. Versin, C. Laisa, A. Prakash, D. Gombeau, G. Van Tendeloo and J-M. Tarascon, *Nat. Mater*., **2015**, *14*, 230.

142 M. Ben Yahai, M. Saubanere ans M-L. Doublet, *Nat. Mater.,* **2019**, *18*, 496.

143 M. Sathiya, G. Rousse, K. Raesha, H. Vesin, M. Sougrati, M-L. Doblet, D.Foix, D. Gonbeau, W. Walker, A. Prakash, M, Ben Hassine, L. Dupont and J-M. Tarascon., *Nat. Mater.,* **2013**, *12*, 827.

144 Y. Xie, M. Saubagnere and M-L ; Doublet, *Energy Environ. Sci.,* **2017**, *10*, 266.

145 J.R. Dahn, E.W. Fuller, M-P. Obrovac, and U. von Sacken, *Solid State Ionics*, **1994**, *69*, 265.

146 M. Guilmard, L. Croguennec, D. Denux and C. Delmas, *Chem. Mater*., **2003**, *15*, 4476.

147 T. Ohzuku, T.yanafawa and M. Kouguchi, *J. Power Sources*, **1997**, *68(1)* 131.

148 M. Guilmard, L. Croguennec and C. Delmas, *Chem. Mater*., **2003**, *15*, 4484.

149 N.Yabuuchi, M. Kajiyama, J. Iwatate, H. Nishikawa, S. Hitomi, R. Okuyama,R. Usui, Y. Yamada and S. Komaba, *Nat. Mater.*, **2012**, *11*, 512.

150 R. Berthelot, D. Carlier and C. Delmas, *Nat. Mater.,* **2011**, *10,* 74.

151 A. Mendiboure, C. Delmas and P. Hagenmuller, *J. of Solid State Chem.*, **1985**, *57*, 323.

152 C. Didier, Guignard, C. Denage, O. Swajwaj, S. Ito, I. Saadoune, J. Darriet C. Delmas, *Electrochem. Solid-State Let.*, 2011,14(5), A75-A78.

153 S-H. Bo, X. Li, A. Toumar, and G. Ceder, *Chem. Mater.,* **2016**, 28, 1419.

154 M. An, E. Gonzalo, M. Casas-Cabanas, *J. Power Sources*, **2014,***258*, 266.

155 L. Vitoux, M. Guignard, M. Suchomel, J. Pramudita, N. Sharma and C. Delmas, *Chem. Mat.,* **2017**, *29*, 7243.

156 M. Radin, S. Hy, M. Sina, C. Fang, H. Liu, J. Vinckeviciute, M. Zhang, S. Whittingham, S. Meng and A. Van der Ven, *Adv. Energy Mater*., **2017**, 1602888.

157 S. Ping Ong, V. Chevrier, G. Hautier, A. Jain, C. Moore, S. Kim, X. Ma and G. Ceder, *Energy Environ. Sci., **2011**, 4, 3680.*

158 J. Molenda, C. Delmas, and P. Hagenmuller, *Solid State Ionics,* **1983**, *9-10*, 431.

159 J. Molenda, C. Delmas, A. Stoklosa and P. Dordor, *Solid State Ionics,* **1984**, *12*, 473.

160 I. Terasaki, Y. Sasago, K. Uchinokura. *Phys. Rev. B Condens Matter Phys.*, **1997**, *56*(20), R12685.

161 K. Takada, H. Sakurai, E. Takayama- Muromachi, F. Izumi, R. Dilanian, T. Sasaki, *Nature*, **2003**,422 (6927), 53.

162 X. Wang, M. Tamaru, M. Okubo and A. Yamada, *J. Phys. Chem. C*, **2013**, *117*, 15545.

163 D. Carlier J-H. Cheng, M. Guignard, M. Yoncheva, B.J. Hwang and C. Delmas, *Dalton Trans.*, **2011**, *40*, 9306.

164 Z. Lu, R. Donaberger and J.Dahn, *Chem. Mater.*, **2000**, *12*, 3583.

165 J-H. Cheng, C-. Pan, J-F Lee, J-M. Chen, M. G. C. Delmas, D. Carlier and B-J. Hwang, *Chem. Mater,* **2014**, *26*, 1219.

166 H. Yoshida, N. Yabuuchi and S. Komaba, *Electrochem Commun.*, **2013**, *34*, 60.

167 R. Stoyanova, D.Carlier, M.Sendova-Vassileva, M.Yoncheva, E. Zhecheva, D. Nihtianova, C. Delmas, J. Solid State Chem. **2010**, *18*, 31372.

168 X. Ma, H. Chen and G. Ceder, *J. Electrochem. Soc.,* **2011**, *158*, A1307.

169 X. Chen, Y. Wang, K. Wiaderek, X. Sang, O. Borkiewicz, K. Chapman, J. Lebeau, J. Lynn and X. Li, *Adv. Funct. Mat.,* **2018**, *28*, 1805105.

170 X. Li, X. Ma, D. Su, R. Chisnell, S. Ping Ong, H. Chen, A. Toumar, J.C. Idrobo, Y. Lei, J. Bai, F. Wang, J. Lynn, Y. Lee and G. Ceder. *Nat. Mater.,* **2014**, *13*, 586.

171 S. Kamakura, Y. Tahara, K. Kubota, K. Chihara and S. Komaba, *Angew. Chem. Int. Ed.,* **2016**, **55**, 12760.

172 N. Yabuuchi and S. Komaba, Sci. Technol. *Adv. Mat.,* **2014**, *15*, 043501.

173 R. Clement, P. Bruce and C. Grey, *J. Electrochem. Soc.*, **2015**, *162*, A2589.

174 N. Yabuuchi, M. Kajiyama, J. Watate, H. Nishikawa, S. Hitomi, R. Okuyama, R. Usui, Y. Yamada and S. Komaba, *Nat. Mat.,* **2012**, *11*, 512.

175 M. Yoncheva, R. Stoyanova, E. Zhecheva, M. Sendova-Vassileva, D. Nihtianova D. Carlier, M. Guignard and C. Delmas, *J. Mater Chem.,* **2012**, *22*, 23408.

176 B. Mortemard De Boisse, D. Carlier, M. Guignard and C. Delmas, *J. Electrochem. Soc.*, **2013**, *160*, A569.

177 J. S. Thorne, R. A. Dunlap and M. N. Obrovac, *J. Electrochem. Soc*., **2013**, *160*, A361.

178 E. Onzalo, M. Han, J.M. Lopez del Amo, M. Casas-Cabanas and T. Rojo, *J. Mater Chem. A.*, **2014**, *2*, 18523.

179 B. Mortemard de Boisse, D.Carlier, M. Guignard, L. Bourgeois and C. Delmas, *Inorg. Chem.*, **2014**, *53*, 11197.

180 E. Talaie, V. Duffort, H. L. Smith, B. Fultzb and L. F. Nazar, *Energy Environ. Sci.*, **2015**, *8*, 2512.

181 M. Kalapsazova, G. Ortiz, J. Tirado, O. Dolotko, E. Zhecheva, D. Nihtianova, L. Mihaylov, and R. Stoyanova, *ChemPlusChem.,* **2015**, *80*, 1642.

182 W. Dose, N. Sharma, J. Pramudita, H. Brand, E. Gonzalo and T. Rojo, *Chem. Mater.,* **2017**, 29, 7416

183 *N.* A. Katcho, J. Carrasco, D. Saurel, E. Gonzalo, M. Han, F. Aguesse and T. Rojo, *Adv. Energ. Mat.,* **2017**, *7*, 1601477.

184 B. Mortemard de Boisse, J-H Cheng, D. Carlier, M. Guignard, J. Pan, S. Bordere, D. Filiminov, C. Drathen, E. Suard, B-J. Hwang, A. Wattiaux and C. Delmas, *J. Mater Chem. A.*, **2015**, *3*, 10796.

185 B. Mortemard de Boisse, D. Carlier, M. Guignard, E. Guerin, M. Duttine, A. Wattiaux and C. Delmas, *Chem, Mater.,* **2018**, 30, 7672.

186 N. Yabuuchi, R. Hara, M. Kajiyama, K. Kubota, T. Ishigaki, A. Hoshikawa, S. Komaba, *Adv. Energ. Mat.,* **2014**, *4*, 1301453.

187 E. de la Lave, E. Talaie, E. Levi, P. Nayak, M.Dixit, P. Tirupathi, P. Hartmann, F. Chesnau, Dan Major, M. Greentein, D. Aurbach and L. Nazar, *Chem.Mater.,* **2016**, *28*, 9064.

188 K. Du, J. Zhu, H. Gao, Y; Li and J. Goodenough, *Energy Environ. Sci.,* **2016**, *9*, 2575.

189 X. Rong, J. Liu, E. Hu, Y. Liu, Y. Wang, J. Wu, X. Yu, K. Page, Y-S Hu, W. Yang, H. Li, X.-Q. Yang, L. Chen and X. Huang, *Joule*, **2018**, *2*, 125.

190 X. Rong, J. Liu, E. Hu, Y. Lu, F. Meng, C. Zhao, X. Wang, Q. Zhang. X. Yu. Lin Gu. Y.-S. Hu, H. Li, X. Huang, X.-Q. Yang, C. Delmas and L. Chen, *Joule*, **2019**, *3*, 1.

191 N. Yabuuchi, R.N Hara, K. Kubota, J. Paulsen and S. Komaba, J. Mater. Chem. A, **2014**, *2*, 16851.

192 U. Maitra, R. House, J. Sommerville, N. Tapia-Ruiz, J. Lozano, N. Guerrini, R. Hong, K. Luo, L. Jin, M. Peres- Osorio, F. Massel, D. Pickup, S. Ramos, X. Lu, D. McNally, A. Chadwick, F. Giustino, T. Schmitt, L. Dida, M. Roberts and P. Bruce, Nat Chem., **2018**, *10*, 288.

193 P. Vassilaras, X. Ma, X. Li, G. Ceder, *J. Electrochem. Soc.,* **2013***, 160,* A207.

194 M. An, E. Gonzalo, M. Casas-Cabanas, *J. Power Sources*, **2014,** *258*, 266

195 B. Mortemard De Boisse, PhD. Thesis Bordeaux, **2014.**

196 J. Paulsen and J. Dahn, *Solid State Ionics*, **1999**, *126*, 3.

197 J. Paulsen, R. Donaberger and J.Dahn, *Chem. Mater.,* **2000**, *12*, 2257.

198 Z. Lu and J Dahn, *J. Electrochem. Soc.*, **2001**, *148*, A 237.

199 Z. Lu, and J. Dahn, *J. Electrochem. Soc*. **2001**, *148*, A1225.

200 D. Lee, J. Xu and S. Meng, *Phys. Chem. Chem. Phys.,* **2013**, *15*, 3304.

201 Y. Zhang, M. Wu, G. Wei, Y. Ling, R. Zhang and Y. Huang, *ACS Cent. Sci.*, **2020**, *6*, 232.

202 S. Komaba, N. Yabuuchi, T. Nakayama, A. Ogata, T. Ishikawa,and I. Nakai, *Inorg Chem.,* **2012**, *51*, 6211.

203 X. Xia and J Dahn*, J. Electrochem. Soc.*, **2012**, *159*, A1048.

204 P.-F. Wang, Y. You, Y.-X. Yin,Y.-G. Guo, *J. Mat. Chem A*, **2016**, *4*, 17660.

205 X. Wang, G. Liu, T. Iwao, M. Okubo and A.Yamada, *J. Phys. Chem. C*, **2014**, *118*, 2970.

206 M. Maazaz, C. Delmas and P. Hagenmuller, *J. Incl. Phenomena*, **1983**, *1*, 45.

207 Y. Wang, X. YU, S. Xu, J. Baai, R. Xiao, Y-S Hu, H. Li, X-Q Yang, L. Chen and X. Huang, Nat. Com *Nat. Com.*, **2013**, *4*, 2858.

208 Y. Wang, R. Xiao, Y-S Hu, M. Avdeev and L. Chen, *Nat. Com.*, **2015**, *6*, 6954.

209 P. Vassilaras, A. Toumar and G. Ceder, *Electr. Chem. Com*. **2014**, *38*, 79.

210 M. Han, E.Gonzalo, G. Singh and T. Rojo, *J. Energy Environ Sci*, **2015**, *8*, 81.

211 D. Yaun, X. Hu, J. Qian, F. Pei, F. Wu, R. Mao, X. Ai, H; Yang and Y. Cao, Electrochem. Acta, **2014**, *116*, 300.

212 I. Hassa, D. Bochholz, S. Passerini, B. Scrosati and J. Hassoun, *Adv. Energy Material*, **2014**, *4*, 1400083.

213 N. Yabuuchi, M. Yano, H. Yoshida, S. Kuze and S. Komaba, *J. Electrochem. Soc.*, **2013**, *160*, A3137.

214 D. Kim, E. Lee, M. Slater, S. Rood and C. Johnson, *Electrochem. Com.,* **2012**, *18*, 66.

215 L. Chagas, D. Buchholz, L Wu, B. Vortmann and S. Passerini, *J. Power Sources,* **2014**, *247*, 377.

216 Y. Zhang, S. Kim, G. Feng, Y. Wang, L. Liu, G. Ceder, and X. Li, *J. Electrochem. Soc.*, **2018**, *165*, A1184.

217 E. Talaie, S. Kim, N. Chen and L. Nazar, Chem. Material. **2017**, *29*, 6684.

218 D. Zhou, F. ZhaO, L. Zhao, W. Huang, X. Kang, Z. Deng, X. Yan, Y. Yu and M. Xiang, Inter. *J. Eletrochem. Sci.*, **2018**, *13*, 2010.

219 X. Wu, J. Guo, D. Wang, G. Zong, M. McDonald and Y. Yang, *J. Power Sources* **2015**, *281*, 18.

220 S. Kumakura, Y. Tahara, S. Sato, K; Kubota and S. Komaba, *Chem. Mater.,* **2017**, *29*, 8958.

221 R. Clement, J. Billaud, A. Amstrong, G. Singh, T. Rojo, P. Bruce, and C. Grey, *Energy Environ. Sci.*, **2016**, *9*, 3240.

222 M. Matsui, F. Mizukoshi and N. Imanishi, *J. Power. Sources*, **2015**, *280*, 205220.

Figures

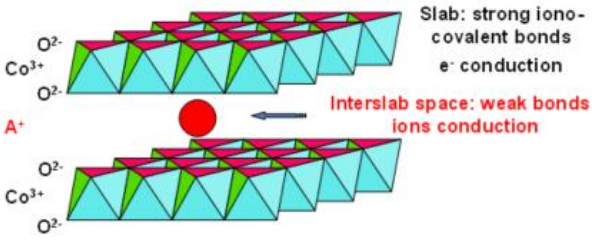

Figure 1. The general structure of a layered oxide

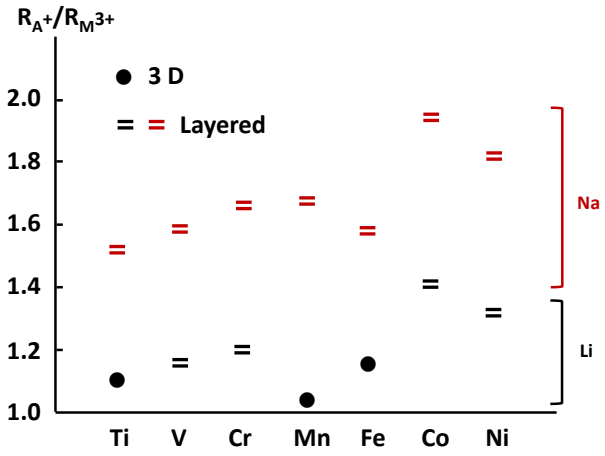

Figure 2. 2D or 3D structures of A_xMO_2 oxides as a function of the cationic radii ratio.

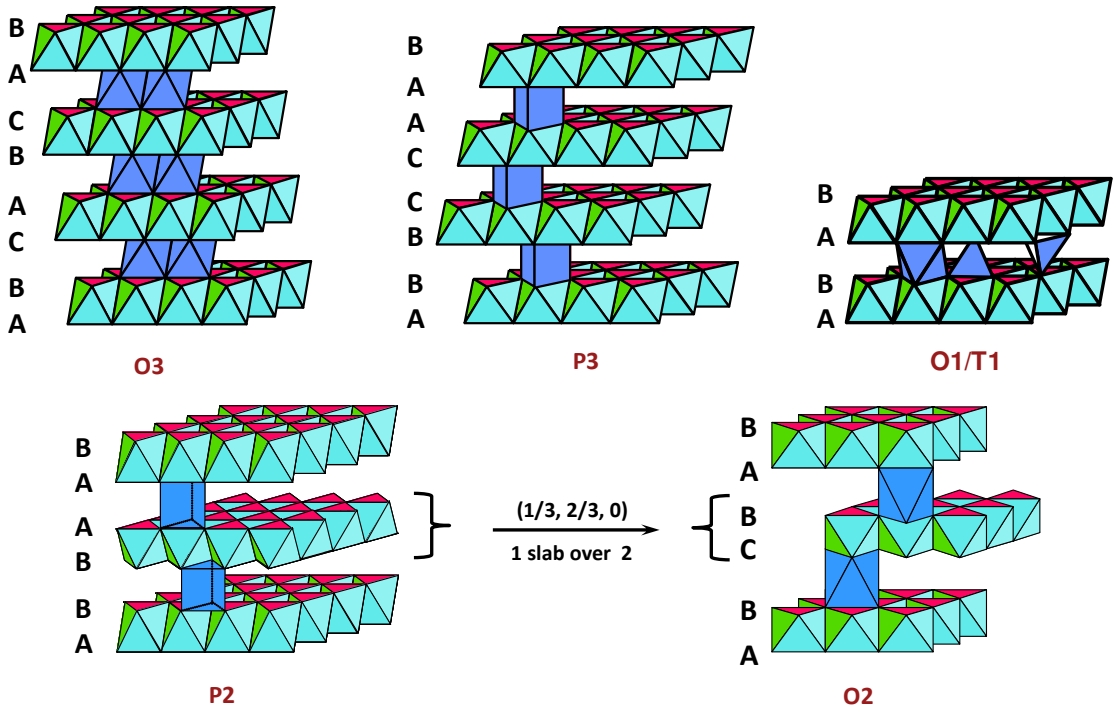

Figure 3. Perspective view of the structures of layered oxides.

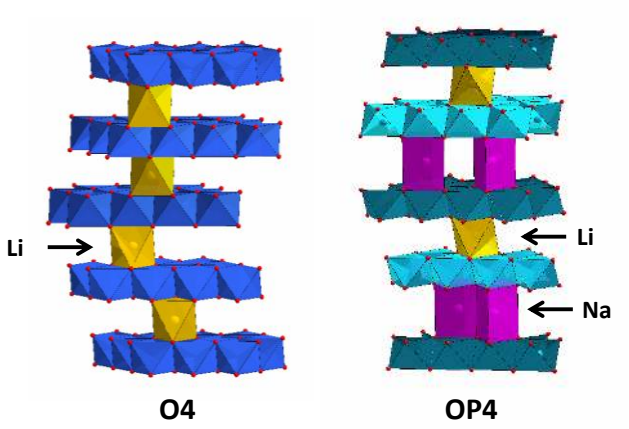

Figure 4. Perspective view of the structures of O4 and OP4 cobalt layered oxides.

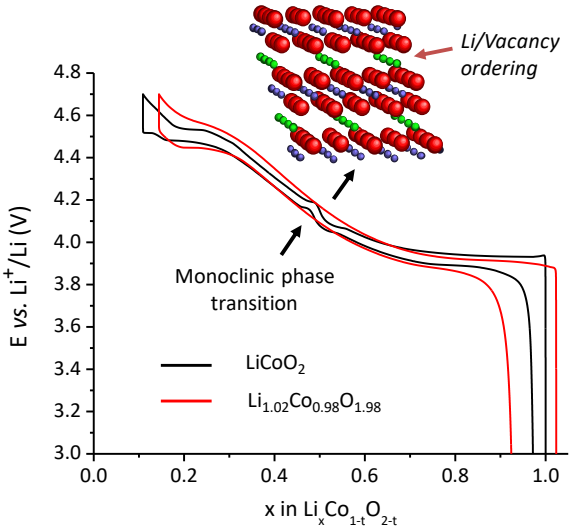

Figure 5. First cycle curve of a Li//Li_xCoO_2 battery. A representation of the structure of $Li_{0.50}CoO_2$ is given in insert.

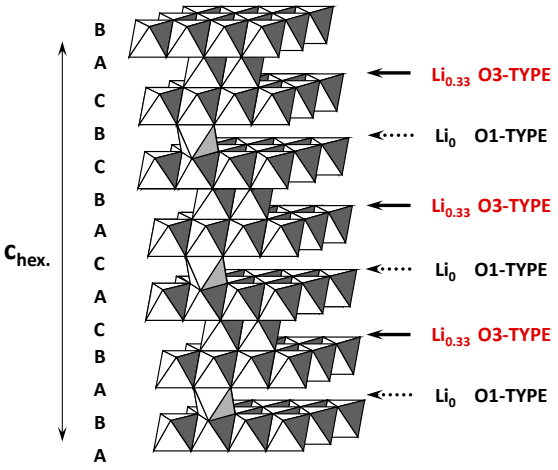

Figure 6. Perspective view of the structure of the $Li_{0.16}CoO_2$ phase.

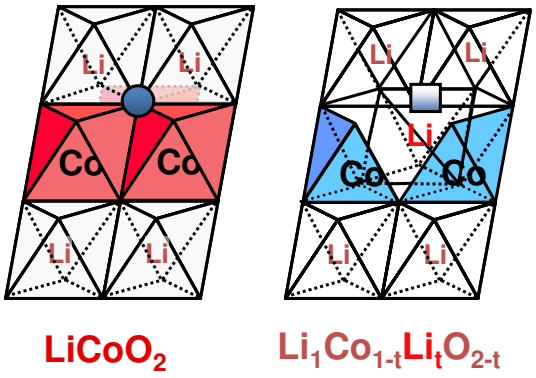

Figure 7. Effect of the presence of Li ions in the cobalt layer of $LiCoO_2$ phases. In the over lithiated phase two IS-Co^{3+} ions are in square pyramidal environment. Adapted with permission. Levasseur S., Ménetrier M. et al. Chem. Mater. 2003, **15,** 348 Copyright 2020, ACS.

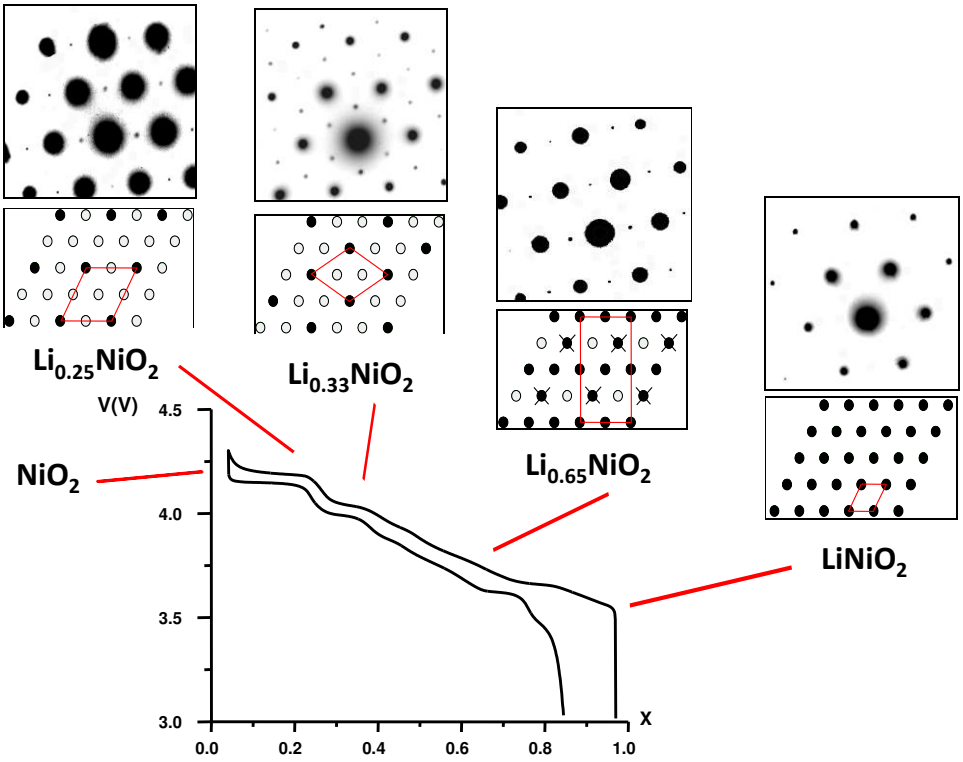

Figure 8. First cycle galvanostatic charge and discharge of a Li // Li_xNiO_2 battery. Electron diffraction and lithium/vacancy ordering for peculiar compositions.

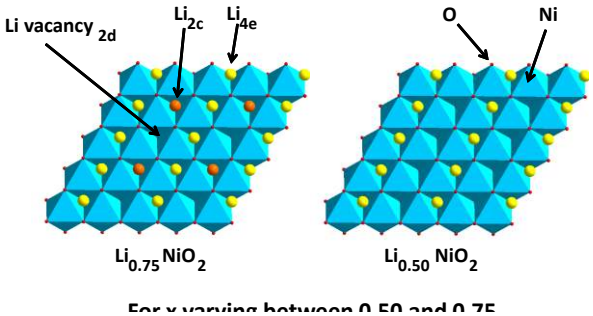

Figure 9. Lithium / vacancy ordering in $Li_{0.50}NiO_2$ and $Li_{0.75}NiO_2$. For x varying between 0.50 and 0.75, the 2c site is progressively occupied.

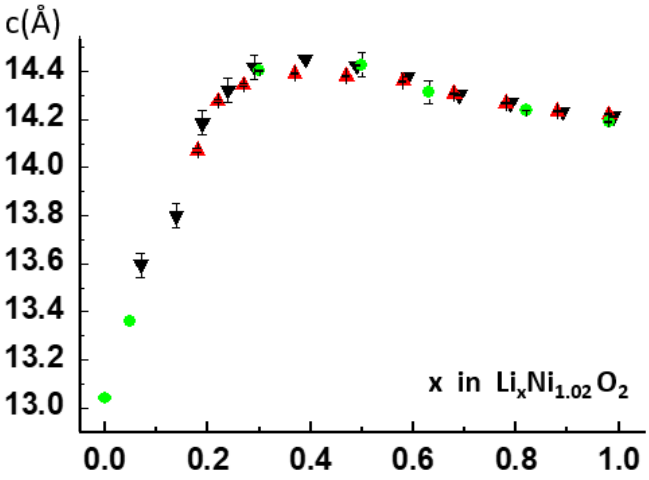

Figure 10. Variation of the $c_{hex.}$ parameter vs the sodium content during the charge of a Li // Li_xNiO_2 battery. The results of several experiments were superimposed.

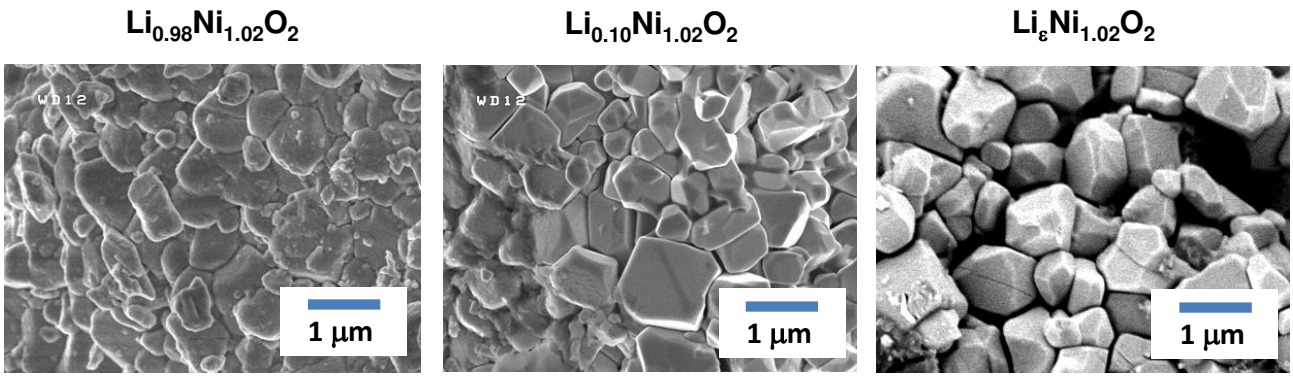

Figure 11. SEM image of $Li_xNi_{1.02}O_2$ phases with various amount of lithium obtained after one cell charge.

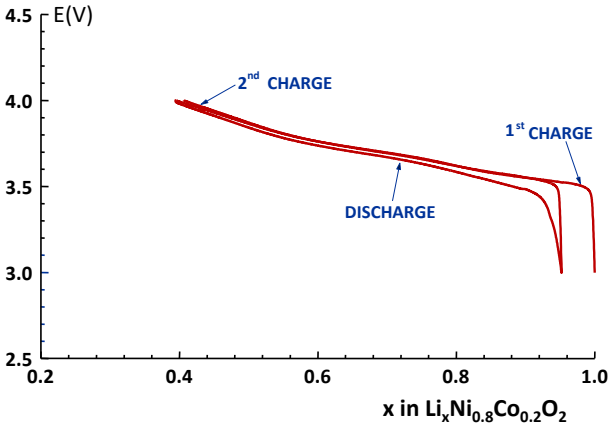

Figure 12. Electrochemical cycling of a Li // $Li_xNi_{0.80}Co_{0.20}O_2$ battery.

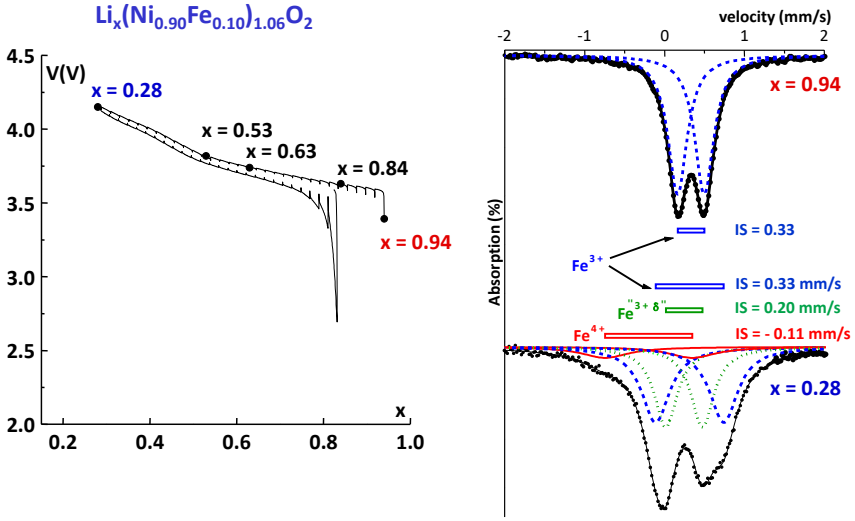

Figure 13. First cycle galvanostatic charge and discharge of a Li// $Li_x(Ni_{0.90}Fe_{0.10})O_2$ battery. For the peculiar compositions indicated on the curves, the Mössbauer spectroscopy shows the iron oxidation.

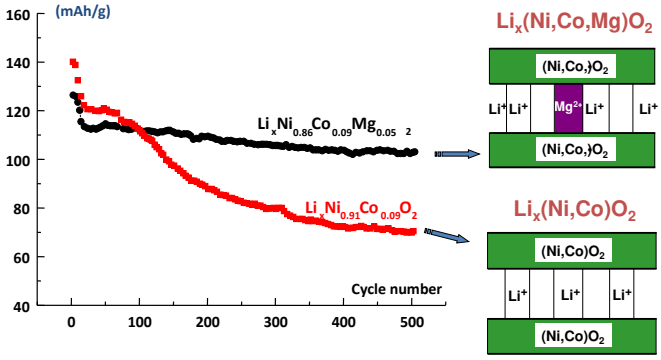

Figure 14. Effect of magnesium on the long range capacity of C//Li(Ni,Co)O_2 batteries. The fading is considerably reduced for magnesium substituted materials. The cationic migration in the lithium layer acts as pillars which reduces the cell parameter changes.

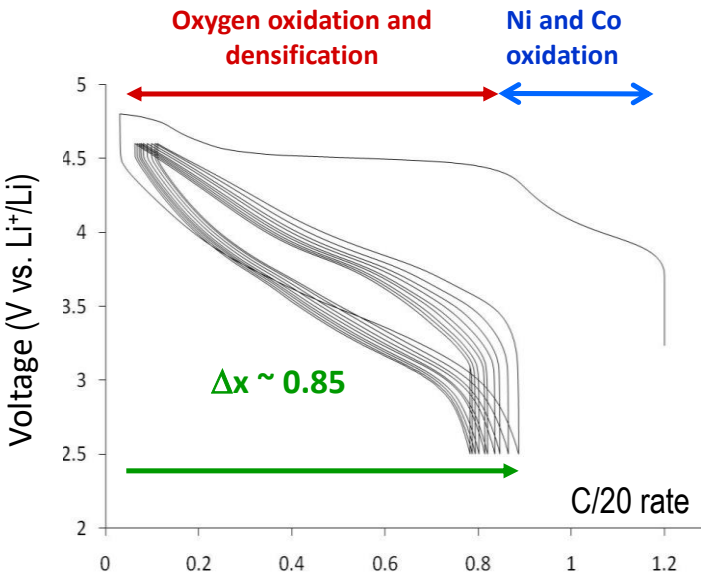

Figure 15. Cycling curve of a Li//$Li_{1.2}Ni_{0.13}Mn_{0.54}Co_{0.13}O_2$ battery. In a first step Ni^{2+} and Co^{3+} ions are oxidized to the tetravalent state. On the 4.6 V plateau O_2 is removed from the surface with material densification. Simultaneously, in the bulk, O^{2-} ions are partially oxidized to $O^{(2-\delta)-}$.

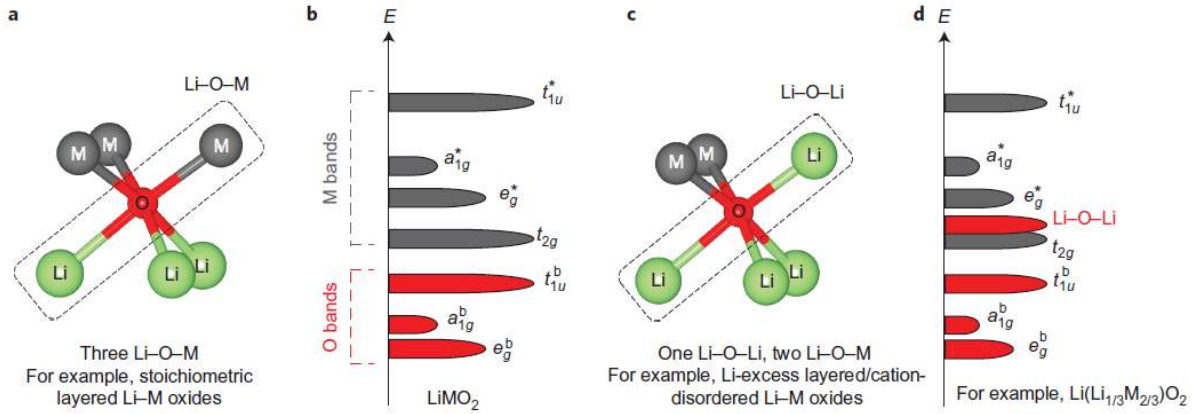

Figure 16. Comparison of the oxygen environment (a,c) and the schematic band structure (b,d) of $LiMO_2$ and $Li(Li_tM_{1-t})O_2$ layered structure. Reproduced with permission of D-H. Seo, J. Lee, A. Urban, R. Malik, S. Kang and G. Ceder, Nat. Chem., **2016**, *8*, 692. Copyrigh 2020, Nature.

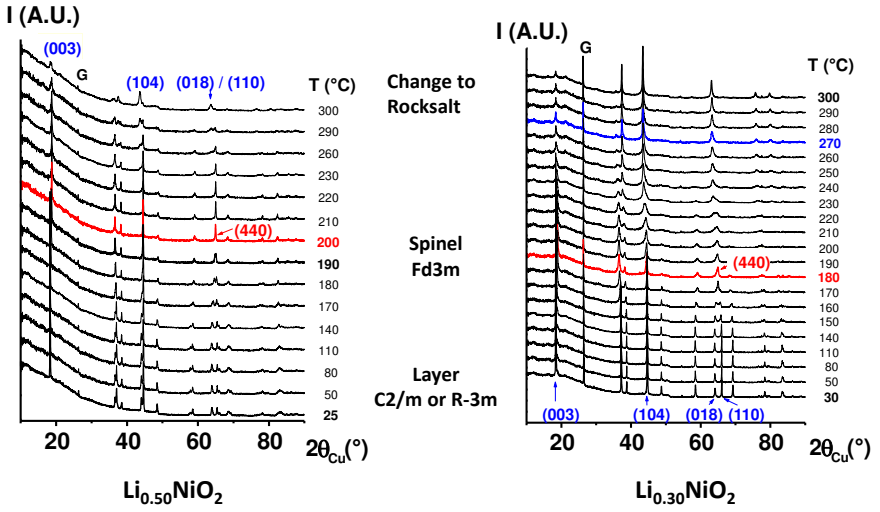

Figure 17. Thermal changes of the XRD patterns of Li_xNiO_2 (x= 0.50, 0.30) phases obtained by electrochemical deintercalation. The transformation from layer to spinel and then two rocksalt is clearly evidenced. Adapted with permission. Guilmard M., Croguennec L. et al. Chem. Mater. 2003, **15,** 4476 Copyright 2020, ACS.

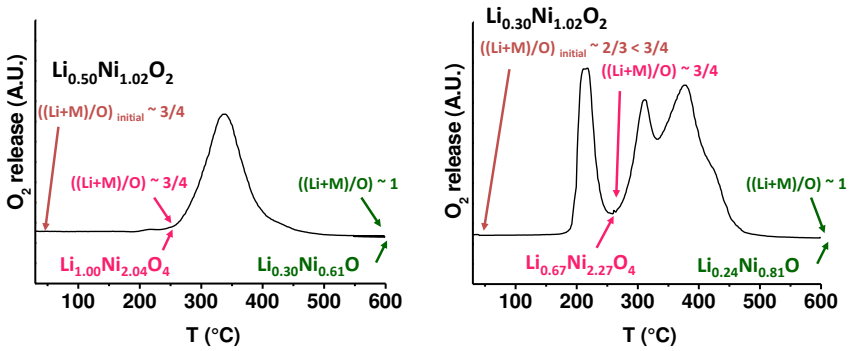

Figure 18. Oxygen evolution during the thermal treatment of Li_xNiO_2 (x= 0.50, 0.30) phases obtained by electrochemical deintercalation. For $Li_{0.50}NiO_2$ the layer to spinel transformation occurs without oxygen evolution. Adapted with permission. Guilmard M., Croguennec L. et al. Chem. Mater. 2003, **15,** 4476 Copyright 2020, ACS.

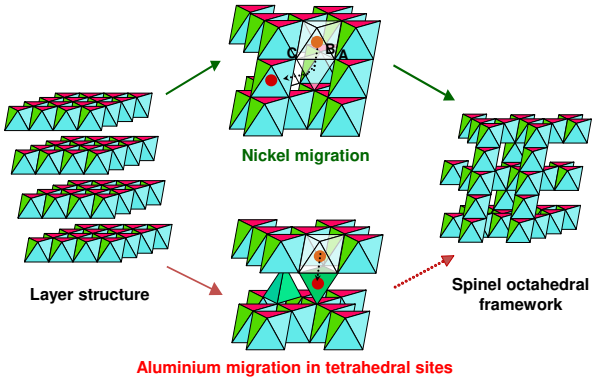

Figure 19. Schematic cationic migration of nickel and aluminum during the layer to spinel transformation.

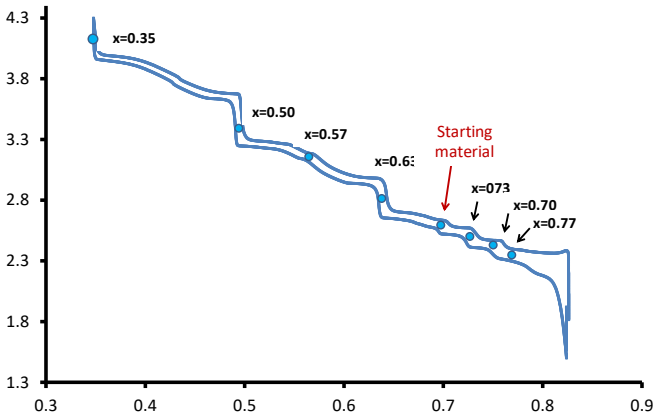

Figure 20. Electrochemical cycling of a Na // P2-Na_xCoO_2 battery.

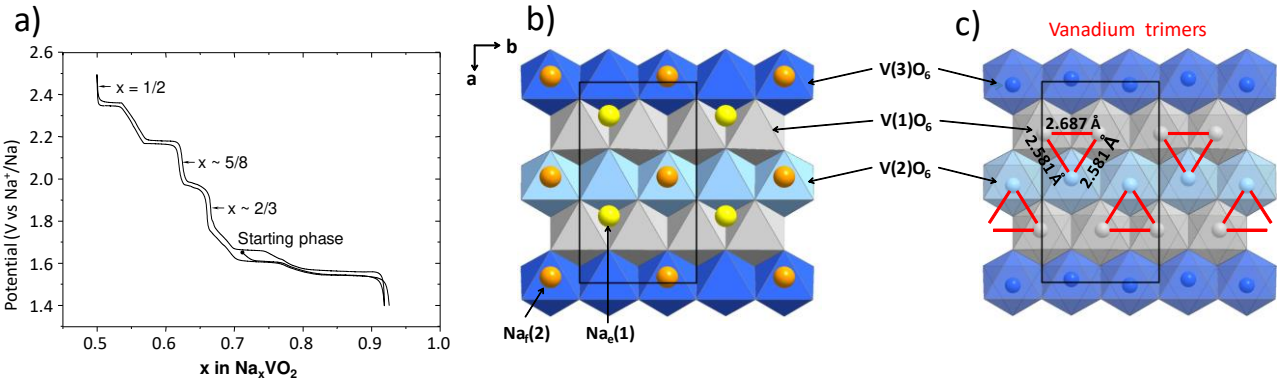

Figure 21. Electrochemical cycling of a Na // P2-Na_xVO_2 battery (a). Structure of the $Na_{1/2}VO_2$ phase obtained by electrochemical deintercalation: sodium ordering in the Na layer (b), formation of vanadium trimers in the VO_2 slab (c). Adapted with permission Guignard M., Didier C. et al., Nat. Mater. 2013, **12,** 74 Copyright 2020, Nature.

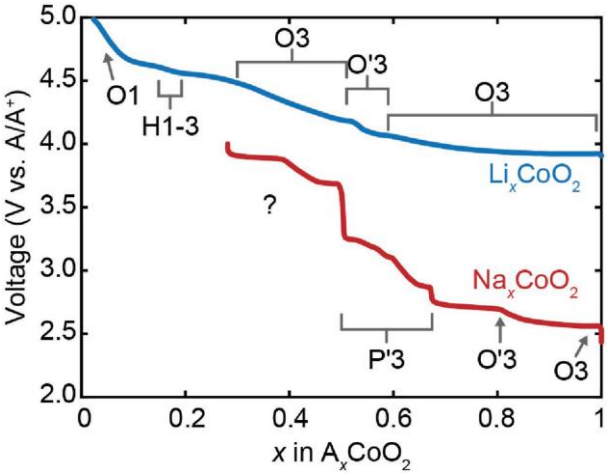

Figure 22. Comparison of the first charge curves of O3-$LiCoO_2$ and O3-$NaCoO_2$. Reprinted from permission of M. Radin, S. Hy, M. Sina, C. Fang, H. Liu, J. Vinckeviciute, M. Zhang, S. Whittingham, S. Meng and A. Van der Ven, *Adv. Energy Mater*. **2017**, 1602888. Copyright 2020, Wiley.

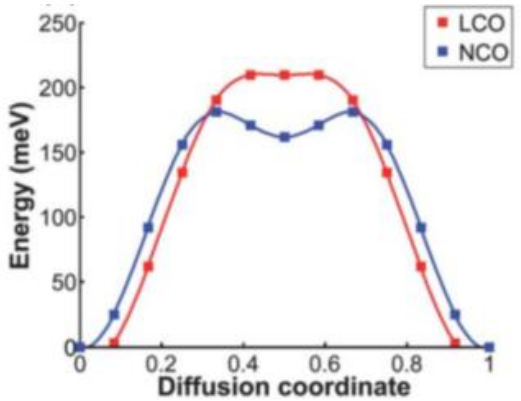

Figure 23. Comparison of calculated diffusion barriers for $LiCoO_2$ (LCO) and $NaCoO_2$ (NCO) with permission S. Ping Ong, V. Chevrier, G. Hautier, A. Jain, C. Moore, S. Kim, X. Ma and G. Ceder, Energy Environ. Sci., **2011**, *4*, 3680. Copyright 2020, RCS.

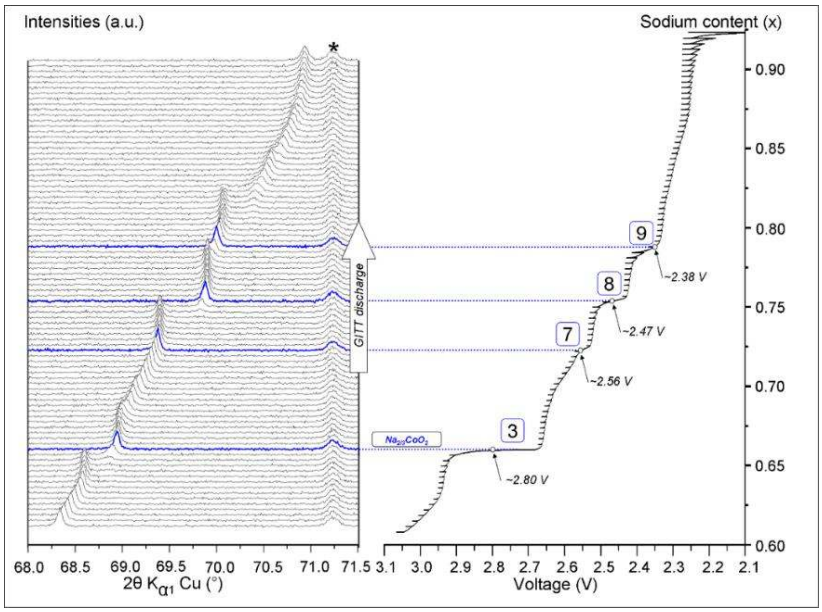

Figure 24. In situ XRD discharge of a P2-Na_xCoO_2 ($x \geq 0.60$) sodium cell. Only the position of the (008) diffraction line is represented. All XRD patterns were recordered after cell relaxation. Adapted with permission Berthelot R., Carlier D. and Delmas C., Nature. Mater. 2011, **10,** 74 Copyright 2020, Nature.

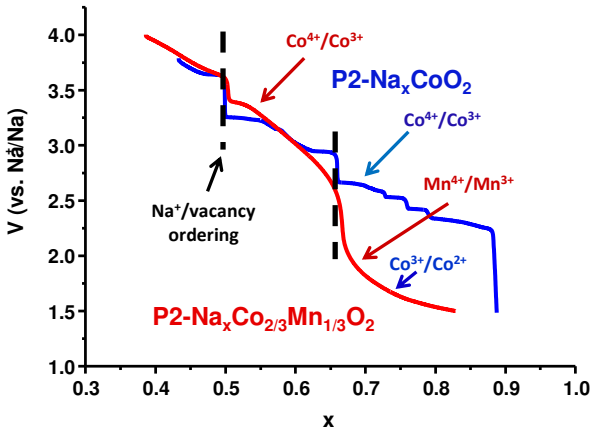

Figure 25. Discharge curves comparison of P2-Na_xCoO_2 and P2-$Na_xCo_{2/3}Mn_{1/3}O_2$ in Na cells. Adapted with permission. Carlier D. Cheng J.H. et al. Dalton Trans 2011, **40,** 9306 Copyright 2020, RCS.

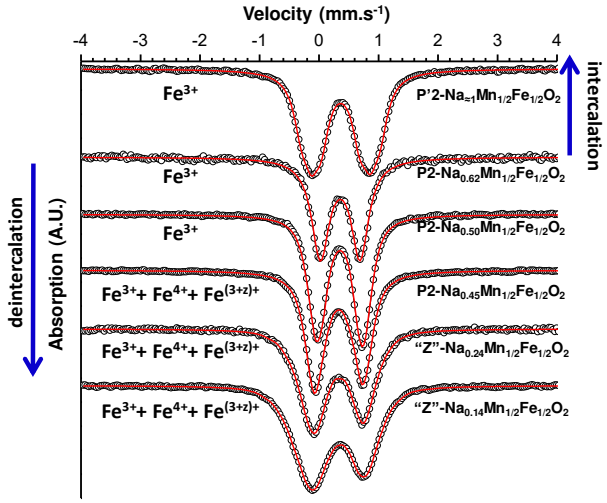

Figure 26. ^{57}Fe Mossbauer spectra of P2-$Na_xMn_{1/2}Fe_{1/2}O_2$ phases obtained by electrochemical Na intercalation and deintercalation from P2-$Na_{0,62}Mn_{1/2}Fe_{1/2}O_2$.

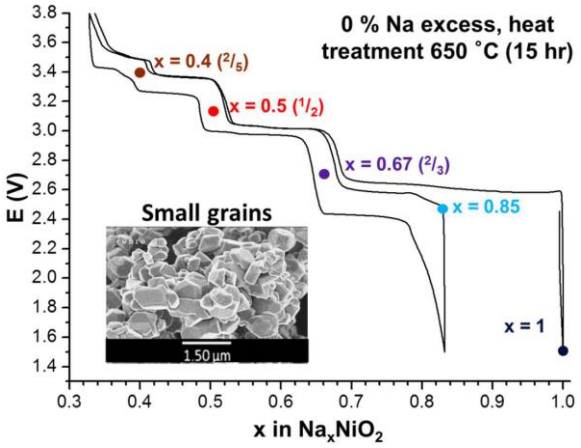

Figure 27. Cycling curve of a Na//$NaNiO_2$ battery.

Table of contents

40 years after the John Goodenough discovery of $LiCoO_2$, which is used in almost all mobile devices, A_xNiO_2 based layered oxides are the most promising material for HV,PHEV and EV (A = Li) and for stationary batteries (A = Na). The great contribution of solid-state chemistry allowed to understand almost all mechanisms involved during the battery cycling and to optimize the material by substitution.

Keywords: Layered oxides, Lithium-ion batteries, sodium-ion batteries, electrode materials

Claude DELMAS, Dany Carlier and M. Guignard

The layered oxides in lithium and sodium-ion batteries: a solid state chemistry approach

ToC